Perigean Spring Tides versus Apogean Spring Tides and their Implication in Pelagic Mixing in the Next 1.4 Billion Years

By: Edwin Alfonso-Sosa, Ocean Physics Education, Started: 24-May-2016, Ended: 3-Jul-2016

Internal waves located north of Aruba, Curacao and Bonaire islands were generated six days earlier by internal tides at St. Lucia and St. Vincent passages during perigean-spring tides on Apr-7-2016.

Abstract

By virtue of the tidal evolution of the Moon's orbit the lunar perigee distance increases at a rate of 3.04 centimeters per year. If we extrapolate this trend 1388 million years in the future it means that the perigee distance will be equivalent to our current lunar apogee distance. On September 13th 2015 and on April 22nd 2016 during apogee-syzygy the semidiurnal tidal accelerations were similar to the expected ones during perigee-syzygy in about 1388 million years into the future. We compared satellite images captured by MODIS on apogee-syzygy with those captured on perigee-syzygy at 8 separate locations widely known to be generation areas of large internal waves. An interesting result was that during the apogee-spring tide we still can have a significant number of detections of internal solitary waves (ISWs). This result can be explained in terms of other astronomical factors (syzygy, zero lunar declination, nodal cycle position) that remained nearly in phase and were sufficient to keep strong semidiurnal tidal currents necessary for the generation of the semidiurnal internal tides. Pelagic mixing will persist for up to one week after apogee-spring tides. Our results suggest that 1388 million years into the future the perigee-spring tides will keep generating internal tides, ISWs and pelagic mixing. Local mixing or abyssal mixing by internal tides will continue to be present 1.4 billion years in the future.

Introduction

The tide force equation is the derivative respect separation distance **r** of the gravitational force between to masses M and **m**, where **G** is the gravitational constant.

$$Gravitational\ force \qquad F = \frac{GMm}{r^2}$$

$$Tide\ force \qquad T = -\frac{dF}{dr}R = \frac{2GMm}{r^3}R$$

$$R: radius\ of\ the\ Earth$$

The separation distance of two celestial bodies is the primary variable in the tidal force equation. The mass of the pair is important but remains secondary. In the tidal force equation the cube of the separation distance dominates the product of the body masses. This is the reason why the Moon tides are stronger than the tides exerted by the gravitational pull of the Sun. The Moon is much closer to us than the Sun, and the lunar tidal acceleration is stronger despite the huge mass of the Sun. The value of the lunar tidal acceleration at the Earth's surface along the Moon-Earth axis is about 1.1 × 10−7 **g**, while the solar tidal acceleration at the Earth's surface along the Sun-Earth axis is about 0.52 × 10−7 **g**, where **g** is the gravitational acceleration at the Earth's surface. The tide-raising force (acceleration) due to the Sun is about 45% of that due to the Moon. When the Moon is closest to Earth, called perigee, the tidal force is stronger. This large tide known as perigee tide or perigean tide repeats itself every 27.55 days (anomalistic month). When the Moon is farthest from Earth, called apogee, the tidal acceleration decreases by about 30% respect its perigee value. Maximum tidal forces in our planet occur when the Sun and the Moon are in conjunction. During inferior conjunction (new moon phase) and superior conjunction (full moon phase) larger tidal accelerations generate two higher tidal bulges in the ocean. This explains why spring tides occur during syzygy. These two tidal bulges manifest as a semidiurnal oscillation in sea level with a period of half a lunar day (12.42 hours). Finally, the angular position of the Sun and the Moon relative to the celestial equatorial plane controls the form of the tidal elevations. The difference between the heights of successive high tides is known as the diurnal inequality. During high lunar declination (tropic tide) the diurnal inequality is larger but during zero lunar declination (equatorial tide) the two heights are equal. From the previous information we can conclude that during the coincidence of perigee-syzygy and zero lunar-solar declinations the oceans will experience the largest semidiurnal tides. Zero solar declinations occur during the spring and autumn equinoxes. The 18.61 year lunar nodal cycle and the 8.85 year cycle of lunar perigee, cause tidal modulations on interannual time scales. The 8.85 perigean lunar cycle has the effect of increasing tidal ranges about every 4.4 years. If the perigee coincides with equinox and the longitude of the lunar node, **N** equals 180 degrees (Minimizing Lunar Declination) they will maximize the semidiurnal form of the tides. N crossed 180° (i.e., lunar declination reached minima) in July 1978, March 1997 and in October 2015 (Haigh et al. 2011). On September 28th 2015 perigee-syzygy, zero lunar declination, and minimum solar declination all coincided. Under these extraordinary circumstances we experienced maximum semidiurnal tidal acceleration and minimum diurnal acceleration. The stronger semidiurnal tidal currents increased the internal wave activity around that day.

Internal (baroclinic) tides are baroclinic waves of tidal period. Internal tides are generated by tidal barotropic flow past seafloor topography. The currents deflected by the topography push the interface several meters from its equilibrium depth and once the current slacks this perturbation is free to propagate along the interface exhibiting a sine waveform. During perigee-syzygy the stronger semidiurnal tidal currents generate a large semidiurnal internal tide that propagates away from the abrupt topography and steepens dramatically producing distinctive solitary wave fronts (Alford et al., 2015) evident in near sun glint images captured by satellite sensors such as MODIS (Christopher Jackson, 2007). When the semidiurnal internal tide dominates, nonlinearity can overcome rotational dispersion, leading to the formation of internal solitary waves (Alford et al., 2015). The internal solitary waves (ISWs) are solitons that can travel hundreds of kilometers across a basin before they break and generate turbulence. In the Caribbean Sea there is strong evidence of ISWs generated during perigee-spring tides that can travel 540 kilometers with speeds around 1.22 m s^{-1} (Alfonso-Sosa, 2012) and impinge the upper slopes of Puerto Rico generating coastal seiches and internal surf 2.3 km seaward of the shelf break (Giese et al., 1982, Giese et al., 1990).

The energy conversion from barotropic tides to internal tides in the deep ocean has been estimated as 1 TW (Egbert and Ray 2000). Internal tides are the primary source of mechanical energy for diapycnal mixing in the deep ocean. Internal tides in the Mona Passage generate a vertical diapycnal diffusivity of O (10^{-3}) m^2 s^{-1} (Alfonso-Sosa et al., 2002). This value is one hundred times larger than in the open ocean away from boundaries or submarine ridges. An internal tidal energetics model of the South China Sea, revealed that the most intense mixing occurs in the deep-water basin with a diapycnal diffusivity of O(10^{-3}–10^{-1}) m^2 s^{-1} within the ~2000-m water column above the seafloor (Wang et al. 2016). This result supports that internal tides are a source of abyssal mixing far away from their local generation area. High values of diapycnal mixing are not confined to the bottom slopes of the generation area but can occur in the abyssal ocean over rough topography such as seamounts, ridges, and reefs. This abyssal mixing is important to keep the deep water oceanic stratification and modulate the Meridional Overturning Circulation (MOC).

As mentioned previously, the 18.61 nodal cycle and the 8.85 perigee cycle are responsible of interannual tidal modulations. In year 2015 the nodal cycle amplified the semidiurnal currents. The same year, specifically on September 28th, the syzygy and perigee coincided incrementing even more the semidiurnal currents. The stronger semidiurnal tidal flow generated a large semidiurnal internal tide that rapidly evolved into ISWs that ended incrementing the mixing. But what happens with the mixing during apogee. Diapycnal mixing by the semidiurnal tide will stop? The Moon's perigee is receding from the Earth at a rate of 30.4 mm/yr and the apogee at a rate of 46.2 mm/year (Williams et al., 2016). How many millions of years will pass before the perigee distance will be too far from Earth to modulate the pelagic mixing? Are planet Earth's oceans condemned to a pelagic mixing crisis far into the future? Is the coincidence between zero lunar declination and syzygy conditions sufficient to keep a strong semidiurnal flow capable to generate large internal tides and pelagic mixing? One easy approach to answer these questions is by taking advantage of the following fact. The perigee distance will increase slowly and in about 1388 million years it will be equal to our current apogee distance. This statement prompts us to put attention into the apogee-syzygy conditions on September 13th 2015 and April 22nd

2016. On both dates the semidiurnal tidal accelerations will be similar to the expected ones during perigee-syzygy about 1388 million years into the future. We compared satellite images captured on apogee-syzygy with those captured on perigee-syzygy in 8 separate locations widely known to be generation areas of large internal waves. The number of detections of ISWs and their duration provided us with a measure of the internal wave activity during apogean-spring and perigean-spring tides. This approach helps us to answer some of these questions.

Methodology

Calculations of Tidal Accelerations and Tidal Currents

Tidal forces were calculated by the computer program called TFHA (Tidal Force and Harmonic Analysis) written by the author on year 2000 at UPRM. Determination of tide-generating forces is based in the Equilibrium Theory of Tides. The formulas used are part from the Manual of Harmonic Analysis and Prediction of Tides, special publication No. 98 U.S. Dept. of Commerce, Coast and Geodetic Survey. Forces or accelerations will be expressed as horizontal and vertical components. The vertical component will be separated into three parts. Quoting from the Manual: "*The first term is independent of the rotation of the earth but is subject to variations arising from changes in declination and distance of the moon. It includes what are known as the long-period constituents, that is to say, constituents with periods somewhat longer than a day and in general a half month or longer. The second term involves the cosine of the hour angle(t) of the moon and this includes the diurnal constituents with periods approximating lunar day. The last term involves the cosine of twice the hour angle of the moon and includes the semidiurnal constituents with periods approximating the half lunar day.*" Each formula was coded into a Matlab script. The positions of the Moon and the Sun were calculated using the formulas from the book titled: Astronomy in the Personal Computer (1994). The formulas were translated from PASCAL to a Matlab script language. The m-file can calculate the year and month when the longitude of the lunar node equals zero degrees (Maximizing Lunar Dec.) and equals 180 degrees (Minimizing Lunar Dec.) Inside the 18.61 year nodal lunar precession cycle. The year and month are accurate but the day has a one-week margin of error. In addition calculates the mean longitude of lunar perigee. The computer program allowed us to find the dates when coincide all the lunar parameters such as perigee-syzygy, zero lunar declination, and when the longitude of the lunar node equals 180°. We found two instances when these parameters are in phase, one in September 2015 and the second on April 2016. These two dates provided us with two independent trials to compare the perigee-spring tides versus the apogee-spring tires. The first trial perigee-syzygy and apogee-syzygy are on September 28th and September 13th 2015, respectively. The second trial perigee-syzygy and apogee-syzygy are on April 7th and April 22nd 2016, respectively.

During the two trial dates the tidal currents regime was dominated by the semidiurnal constituents: M2, S2, N2, K2. The barotropic semidiurnal tidal velocities were obtained from the regional solutions for the Caribbean Sea, the Amazonian Shelf, Indonesian seas, Bay of Bengal and China Sea from the Oregon State University (OSU) inverse barotropic tidal model (OTIS)(Egbert et al. 1994; Egbert and Erofeeva 2002) with 1/30 degree spatial resolution. http://volkov.oce.orst.edu/tides/region.html

The tidal currents were predicted using the Tidal Model Driver (TMD) MATLAB toolbox created by scientists at Earth Space Research (http://polaris.esr.org/ptm_index.html).

Tele detection of Internal Waves

In the last decade, 250-m resolution MODIS images acquired by the Earth Observing System Terra and Aqua Satellites during sunglint conditions allowed us to survey high-frequency nonlinear internal solitary wave occurrences on a near-global scale (Christopher Jackson, 2007). It is possible to detect internal solitons packets leaving the generation area during fortuitous conditions: minimum cloud cover, near-specular reflectance pattern of sunlight off the ocean surface (sun glint) and strong oceanic stratification. The origin and speed of internal solitary waves in the Caribbean Sea and in the Western Equatorial Atlantic Ocean had been determined by analysis of MODIS images (Alfonso-Sosa, 2013; Alfonso-Sosa, 2013). Each trial consists of a 9-day window around the astronomical event. Two satellites passes each day give us a total of 18 opportunities to detect internal waves. Cloudiness, no-sunglint conditions, no satellite coverture of the area of interest reduced detections opportunities.

Results

Tidal Accelerations and Tidal Currents

On September 28th 2015 (YD 270) the coincidence of the lunar parameters: full moon phase, perigee (356075 km) and zero lunar declination maximized the range of the total vertical lunisolar acceleration (Figure 2 top). On the same day the total vertical lunisolar acceleration, the vertical long-term lunar acceleration and the vertical semidiurnal lunar acceleration attained their maximum values (Figure 2 bottom). In contrast, the vertical diurnal lunar acceleration show their minimum value. The maximum value of the long-term lunar acceleration was 2.77E-08 **g**. This perfect alignment of the lunar parameters allowed for a maximum vertical semidiurnal lunar acceleration of 9.8E-08 **g** at the expense of its diurnal counterpart. On year 2015 the M2 *f*-factor was the largest. Specifically, on YD 270 the four semidiurnal constituents: M2, S2, N2 and K2 were perfectly in phase (Figure 3 bottom). Fifteen days before YD 270, on September 13th (YD 255.3) the semidiurnal constituents M2 and S2 were in phase but the other two constituents N2 and K2 were not (Figure 3 top). They were out of phase because on that day the new moon coincided with the apogee (405607 km). The N2 constituent responds to the perigee-apogee cycle (Figure 2 Top). The next day (YD 256.1) the lunar declination was zero. As expected, the vertical long-term lunar acceleration and vertical semidiurnal lunar acceleration (7.0E-08 **g**) values were smaller than the ones corresponding to September 28th (YD 270). Both dates have in common a syzygy-equatorial (near zero lunar declination) condition but they differ extremely in geocentric distance, from perigee to apogee exactly 49532 km, this is equivalent to a percentage change of 13.9%. The change from perigee-syzygy to apogee-syzygy represents a decrease in vertical semidiurnal lunar acceleration of -2.8E-08 **g**; this is equivalent to a percentage change of -28.8%. The decrease in semidiurnal lunar acceleration reduces the semidiurnal tidal currents. Figure 4 shows a time series of the semidiurnal currents at St. Lucia Passage (top) and St. Vincent Passage (bottom) starting on September 14th 2015 and ending on October 2nd 2015. From perigee-syzygy (14.7 days since start date) to apogee-syzygy (0.2127 days since start time) the maximum current speed at St. Lucia Passage and St. Vincent Passage was reduced by 6

cm/s and 4.9 cm/s, respectively. This represents a percentage change of -25.6% and -24.0% in the maximum speed of the currents (see Table 2). Assuming a squared dependence between the speed of the currents and ocean mixing we calculated the percentage change from squared perigee-spring currents to squared apogee-spring currents. For St. Lucia Passage and St. Vincent passage the values were -44.6% and -44.2%, respectively (Table 2). These percentages suggest a considerable reduction in ocean mixing when perigee-spring currents are compared with apogee-spring currents.

On April 2016 we had another chance to compare the perigee-syzygy versus apogee-syzygy conditions. On April 7th 2016 (YD 97.5), new moon phase and perigee (357009 km) coincided but this time zero declination occurred one day before (Figure 5 top). The alignment of the semidiurnal constituents were not perfect as in September 28th 2015 (compare Figure 6 top with Figure 3 bottom) but was good enough to show a maximum vertical semidiurnal lunar acceleration value of 9.7E-08 **g** on YD 97.04 (Figure 5 bottom). The maximum value of long-term lunar acceleration was 2.75E-08 **g** similar to the observed on September 28th 2015. The perigee-syzygy conditions on both days were similar. During apogee-syzygy conditions that occurred on April 22nd 2016 the maximum vertical semidiurnal lunar acceleration value was 6.5E-08 **g**. This value was a little bit smaller than the one corresponding to September 13th 2015 despite having the same apogee distances. This small difference is attributed to the fact that N2 and K2 were out of phase. In other terms, the lunar declination on April 22nd was not zero (-6.5°) during apogee. This time the percentage change from perigee to apogee semidiurnal lunar acceleration was -33.0% (Table 2). Based on the two present cases, we can say that the percentage change in vertical semidiurnal lunar acceleration from perigee-syzygy to apogee-syzygy conditions runs between a -29% to -33%. Comparing the perigee-spring versus the apogee-spring maximum current speeds at St. Lucia Passage and St. Vincent Passage (Figure 7) we observe a reduction by 6.6 cm/s and 5.3 cm/s, respectively. This represents a percentage change of -28% and -26.4% in the maximum speed of the currents at each location. The corresponding reductions in ocean mixing were -48.1% and -45.8%, respectively. These values are similar to the observed ones on September 2015 at the same locations.

The previous exercise was repeated exactly for 9 locations in tropical seas where semidiurnal currents impinging on abrupt submarine topography are responsible for the generation of internal tides and large internal solitary waves. Table 2 details each percentage change from maximum perigee-spring current to maximum apogee-spring current. The largest change was at Lombok Strait and St. Lucia Passage (Figure 8). The smallest change was at Sibutu Passage. The average percentage change on September 2015 was -22.0 ± 2.1% and on April 2016 was -25.5 ± 2.1%. This means that there is a reduction of not less than 15% and not more than 30% from maximum perigee-spring currents to maximum apogee-spring currents in the tropical seas. The average percentage change from squared perigee-spring currents to squared apogee-spring currents on September 2015 was -39.2 ± 3.3 % and on April 2016 was -44.4 ± 3.1 %.

Maps of the velocity of the M2 semidiurnal barotropic currents are shown in Figures 9 to 13. Each one shows the main velocity component responsible for the forcing of internal waves at each of the selected locations. These maps show the exact generation site (marked with a black circle) and its surrounding dissipation region.

Detection of Internal Waves by MODIS

Figures 14 to 18 show internal waves generated at these same locations between September 27th and October 1st 2015. These images captured by the MODIS sensor confirmed that around the time of perigee-syzygy (September 28th) internal waves were generated from those locations. No internal waves were detected at the generation sites during moon quarter phase or quadrature.

Comparing MODIS images captured inside a 9-day window around perigee-spring tide (26 September 2015-4 October 2015) versus around apogee-spring tide (9-17 September2015) revealed that the first detection of internal waves occurred between one day before and two days after the perigee or apogee event. The last detections occurred 4 days after apogee and 6 days after perigee (Table 3). Figure 19 (top) shows a pattern of a greater number of detections during perigee than during apogee. In a second trial, images captured inside a 9-day window around perigee-spring tide (4-12 April 2016) versus apogee-spring tide (19-27 April 2016) revealed similar number of detections at the same locations (Figure 19, bottom). Surprisingly, six of the eight locations show equal or higher number of detections around apogee-spring tide rather than around perigee-spring tide. When we compared number of detections around perigee-spring tides for both trials we found that five of the eight locations show a higher number of detections in the first trial. Figure 20 shows the elapsed days between last and first detection around perigee-spring tides versus apogee-spring tides. The first and second trials show equal or longer elapsed days during perigee-spring tides in six and five locations, respectively.

Discussion

On September 28th under extraordinary circumstances of simultaneous perigee and full moon phase- separated by just half an hour- during zero lunar declination, and all happening in the year 2015 when the 18.8-years nodal cycle maximizes the semidiurnal acceleration; the conjunction of all these astronomical factors forced perigee-spring tides with strong semidiurnal currents and the generation of large internal semidiurnal tides at eight different locations in the tropical oceans. The evolution of the internal tides into packets of internal solitary waves (ISWs) allowed MODIS to detect the start and end dates of the increased internal wave activity. ISWs first appeared one to two days around the perigee-syzygy event and can still be detected far from the generation site about 7-8 days later. This result sustains that the dissipation of large amplitude internal tides by means of ISWs and pelagic mixing can persist in the basin for up to one week. An interesting result was that during the apogee-spring tide we can still have a significant number of ISWs detections. This result can be explained in terms that the other astronomical factors (syzygy, zero lunar declination, nodal cycle position) remained nearly in phase and were sufficient to keep strong semidiurnal tidal currents necessary for the generation of the internal tides. We should too expect that pelagic mixing will persist for up to one week after apogee-spring tides but in average is about 5 days. The percentage change in vertical semidiurnal lunar acceleration from perigee-syzygy to apogee-syzygy condition runs between -29% to -33% causing a percentage change of -22% and -26% when going from maximum perigee-spring currents to maximum apogee-spring currents. These percentages were not large enough to suppress the generation of ISWs at most of the selected locations. Despite that fact, we had more detections of ISWs around perigee-spring

tides than around apogee-spring tides in most locations. We should expect that pelagic mixing persists up to one week after the occurrence of perigee-spring currents in most examined locations.

Implications on the Future of Pelagic Mixing

Our results revealed the presence of significant activity of internal waves during apogee-syzygy conditions. The generation of packets of ISWs is an essential part in the pelagic mixing process. The ISWs travel hundreds of kilometers before impinging on submarine topography and break. The internal wave breaking at the upper slope generates mixing and turbulence. This means that the fate of ISWs is to increase the pelagic mixing. Generated by strong semidiurnal tidal currents even at apogee distances (405607 km) guarantees significant pelagic mixing during apogee-syzygy. The Moon's perigee distance from Earth increases at a rate of 3.04 cm/yr. At this rate the perigee distance will increase slowly and in about 1388 million years it will be equal to our current apogee distance. Figures 21-22 show a projection of the apogee and perigee tidal accelerations; again it will take about 1388 million years to experience a perigee tidal acceleration equal to our current apogee tidal acceleration. Inside the 1388 million years timespan perigee-syzygy conditions will still show tidal acceleration capable to generate internal waves and pelagic mixing. The dissipation of internal tides will still be an effective wave to loose tidal energy. It is unclear how the configuration of the ocean bathymetry will be on hundreds of millions of years but new ISWs generation and dissipation's locations will exist.

References

Alfonso-Sosa, E., 2013. First MODIS Images Catalog of Aves Ridge Solitons in the Caribbean Sea (2008-2013) 32 pp. 8.92 MB PDF.

Alfonso-Sosa, E., 2013. MODIS Images Catalog of Ceará Solitons Located Offshore of the Amazon River Delta in the Equatorial Atlantic Ocean (2013). PDF

Alfonso-Sosa, E., 2012. Estimated Speed of Aves Ridge Solitons Packets by Analysis of Sequential Images from the Moderate Resolution Imaging Spectroradiometer (MODIS) 11 pp. 2.55 MB PDF.

Alfonso-Sosa, E., Capella J. E., Morell J., Lopez J. M., Dieppa A., and Marvi Teixeira, 2002. COASTAL SEICHES, INTERNAL TIDE GENERATION, AND DIAPYCNAL MIXING OFF PUERTO RICO. https://www.academia.edu/9814302/COASTAL_SEICHES_INTERNAL_TIDE_GENERATION_AND_DIAPYCNAL_MIXING_OFF_PUERTO_RICO

Alford, M. H., and Coauthors, 2015: The formation and fate of internal waves in the South China Sea. Nature, 521, 65–69, doi:10.1038/nature14399.

Christopher Jackson, 2007. Internal wave detection using the Moderate Resolution Imaging Spectroradiometer (MODIS). JOURNAL OF GEOPHYSICAL RESEARCH, VOL. 112, C11012, doi:10.1029/2007JC004220.

Chapman, D. C., Giese, G. S., 1990. A model for the generation of coastal seiches by deep-sea internal waves. Journal of Physical OceaEgbert, G. D., and R. D. Ray, 2000: Significant dissipation of tidal energy in the deep ocean inferred from satellite altimeter data. Nature, 405, 775–778, doi:10.1038/35015531.

Egbert, G. D., and R. D. Ray, 2000: Significant dissipation of tidal energy in the deep ocean inferred from satellite altimeter data. Nature, 405, 775–778, doi:10.1038/35015531.

Egbert, G. D., and S. Y. Erofeeva, 2002: Efficient inverse modeling of barotropic ocean tides. J. Atmos. Oceanic Technol., 19, 183–204, doi:10.1175/1520-0426(2002)019,0183:EIMOBO.2.0.CO;2.

Giese, G.S., Chapman, D.C., Collins, M. G., Encarnacion R., Jacinto G., 1998. The Coupling between Harbor Seiches at Palawan Island and Sulu Sea Internal Solitons. Journal of Physical Oceanography 28, 2418-2426.

Giese, G.S., Chapman, D.C., Black, P.G., Fornshell, J.A., 1990. Causation of large-amplitude coastalseiches on the Caribbean coast of Puerto Rico. Journal of Physical Oceanography 20, 1449-1458

Giese, G. S., Hollander, R.B., Francher, J.E., Giese, B.S., 1982. Evidence of coastal seiche excitation by tide-generated internal solitary waves, Geophysical Research Letters 9, 1305-1308

Haigh, I. D., M. Eliot, and C. Pattiaratchi (2011), Global influences of the 18.61 year nodal cycle and 8.85 year cycle of lunar perigee on high tidal levels, J. Geophys. Res., 116, C06025, doi:10.1029/2010JC006645.

Wijeratne, E. M. S., Woodworth, P. L. y D. T. Pugh, 2010. Meteorological and internal wave forcing of seiches along the Sri Lanka Coast. Journal of Geophysical Research 115, C03014. 1-13.

OLIVER MONTENBRUCK and THOMAS PFLEGER, 1994. ASTRONOMY IN THE PERSONAL COMPUTER, Vol. 1, Springer-Verlag, 312 pp.

Schureman,P.,1958: Manual of Harmonic Analysis and Prediction of Tides, Special Publication No. 98 Revised (1940) Edition, U.S. Dept. of Commerce, Coast and Geodetic Survey, 317 pp.

Wang X., Peng S., Liu Z., Huang R. X., Qian Y., and Y. Li, 2016. Tidal Mixing in the South China Sea: An Estimate Based on the Internal Tide Energetics. JPO Vol. 46: Issue. 1: Pages. 107-124. DOI: 10.1175/JPO-D-15-0082.1

Williams J. G., D. H. Boggs, and J. Todd Ratcliff, 2016. LUNAR TIDAL RECESSION. 47th Lunar and Planetary Science Conference (2016).

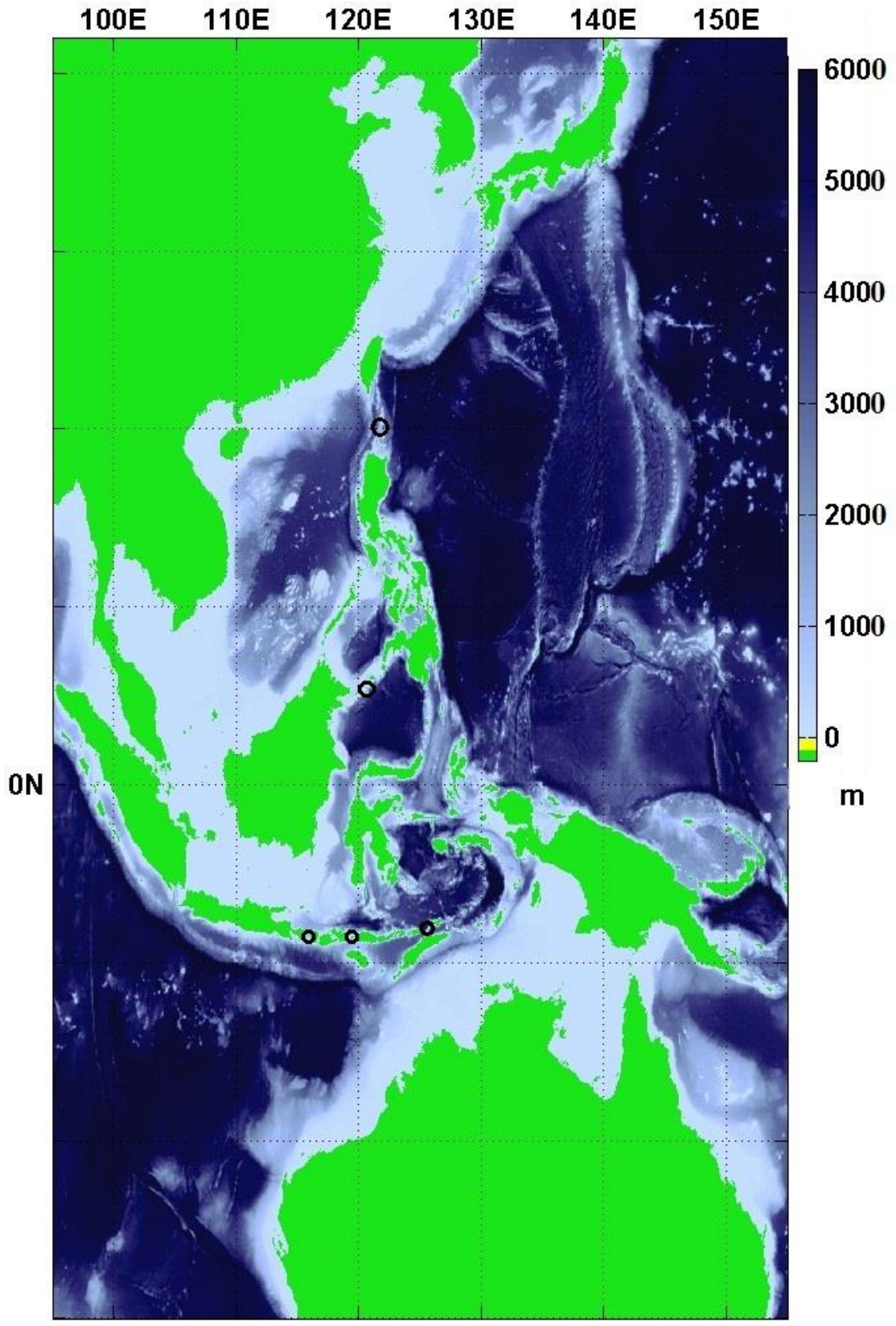

Figure 1- Bathymetric Map of the Indonesian Straits, the Sibutu Strait and the Luzon Strait, Black Circles.

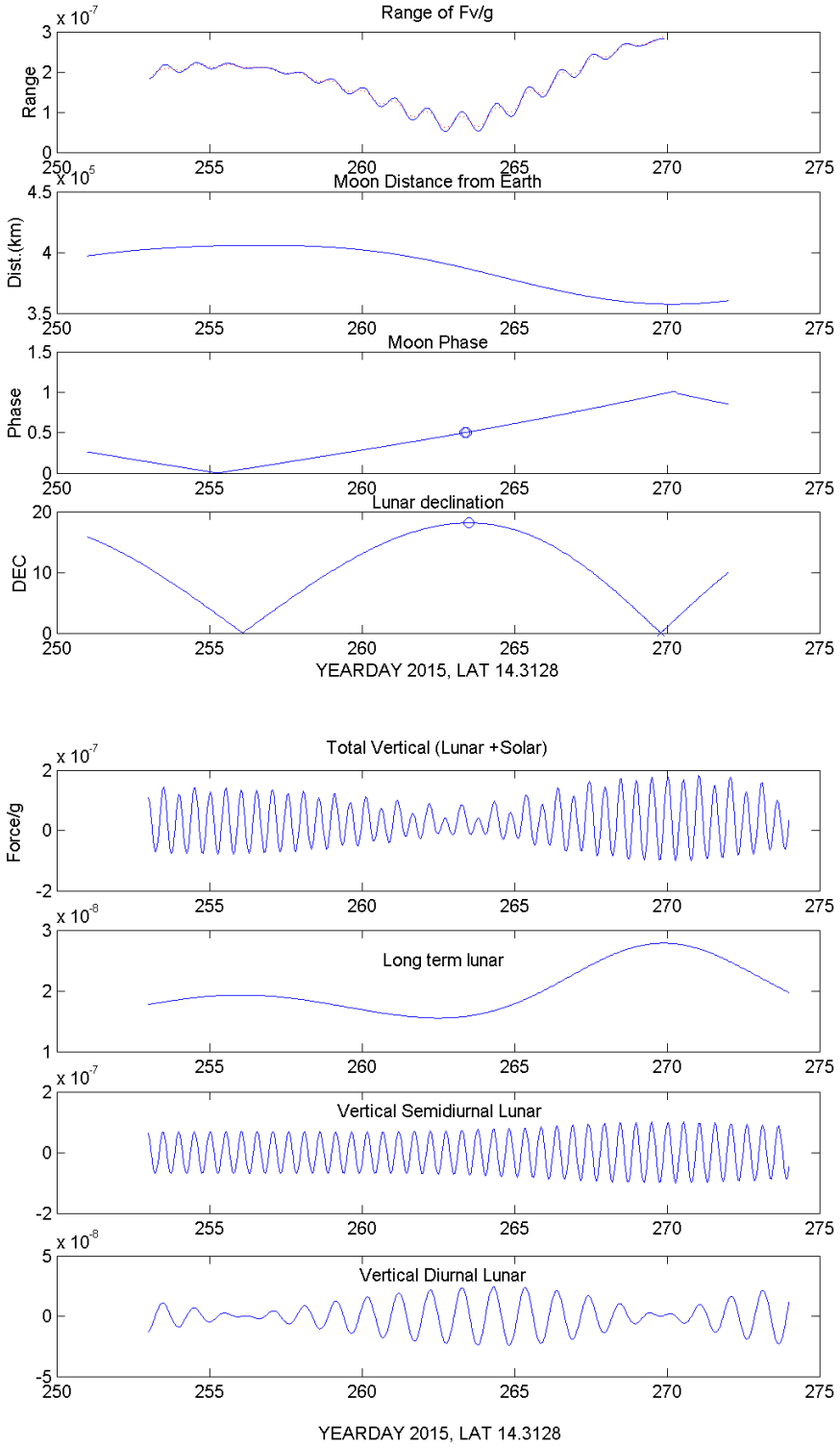

Figure 2 – (Top) Range of the total vertical luni-solar acceleration, Geocentric Moon's distance from Earth, Moon's phase and lunar declination. (Bottom) Total vertical luni-solar acceleration, vertical long-term lunar acceleration, vertical semidiurnal lunar acceleration and vertical diurnal lunar acceleration.

Table 1. Time of syzygy and perigee expressed in year days (YD), the geocentric perigee distance, the maximum vertical semidiurnal lunar acceleration, and the percentage change from perigean to apogeal semidiurnal acceleration at St. Lucia Passage.

Location	Phase	YD	Moon's Position	YD	Date	Dist (km)	YD	Date	Maximum Vertical Semidiurnal Lunar Aceleration /g	Percentage Change from Perigean to Apogee SD Lunar Aceleration (%)
St. Lucia Passage	Full Moon	270.23	Perigee	270.21	9/28/15 4:59	356075	270.03	9/28/15 0:37	9.8E-08	
St. Lucia Passage	New Moon	255.27	Apogee	255.29	9/13/15 7:03	405607	255.54	9/13/15 12:59	7.0E-08	-28.8
St. Lucia Passage	New Moon	97.48	Perigee	97.51	4/7/16 12:15	357009	97.04	4/7/16 0:57	9.7E-08	
St. Lucia Passage	Full Moon	112	Apogee	112.00	4/22/16 0:00	405607	111.52	4/21/16 12:29	6.5E-08	-33.0
									Edwin Alfonso-Sosa, 2016	

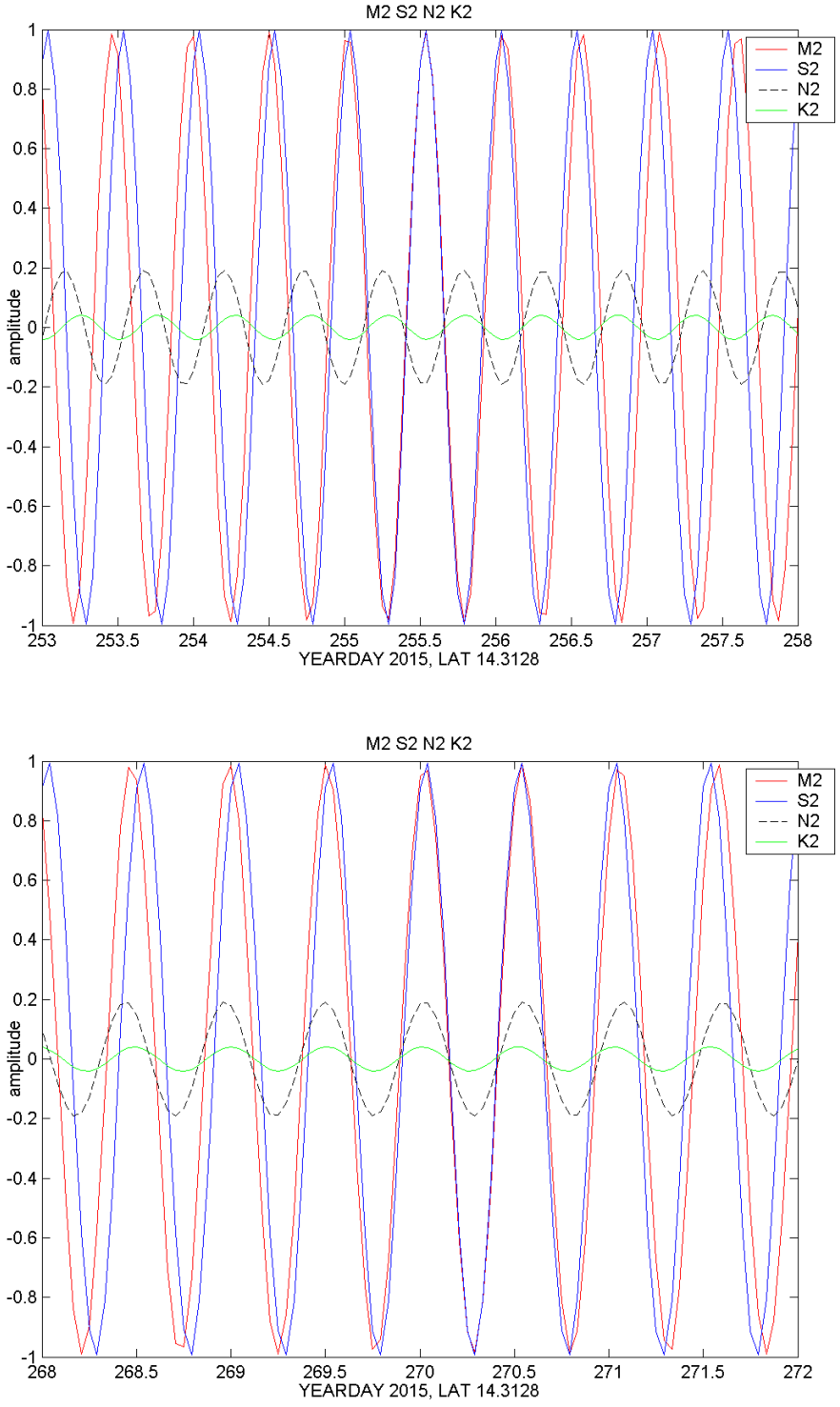

Figure 3- The semidiurnal constituents of the vertical acceleration. The amplitudes were normalized for an easy comparison. The year day 255.5 and 270 of 2015 are equivalent to 13-SEP-2015 12:00 and 28-SEP-2015, respectively.

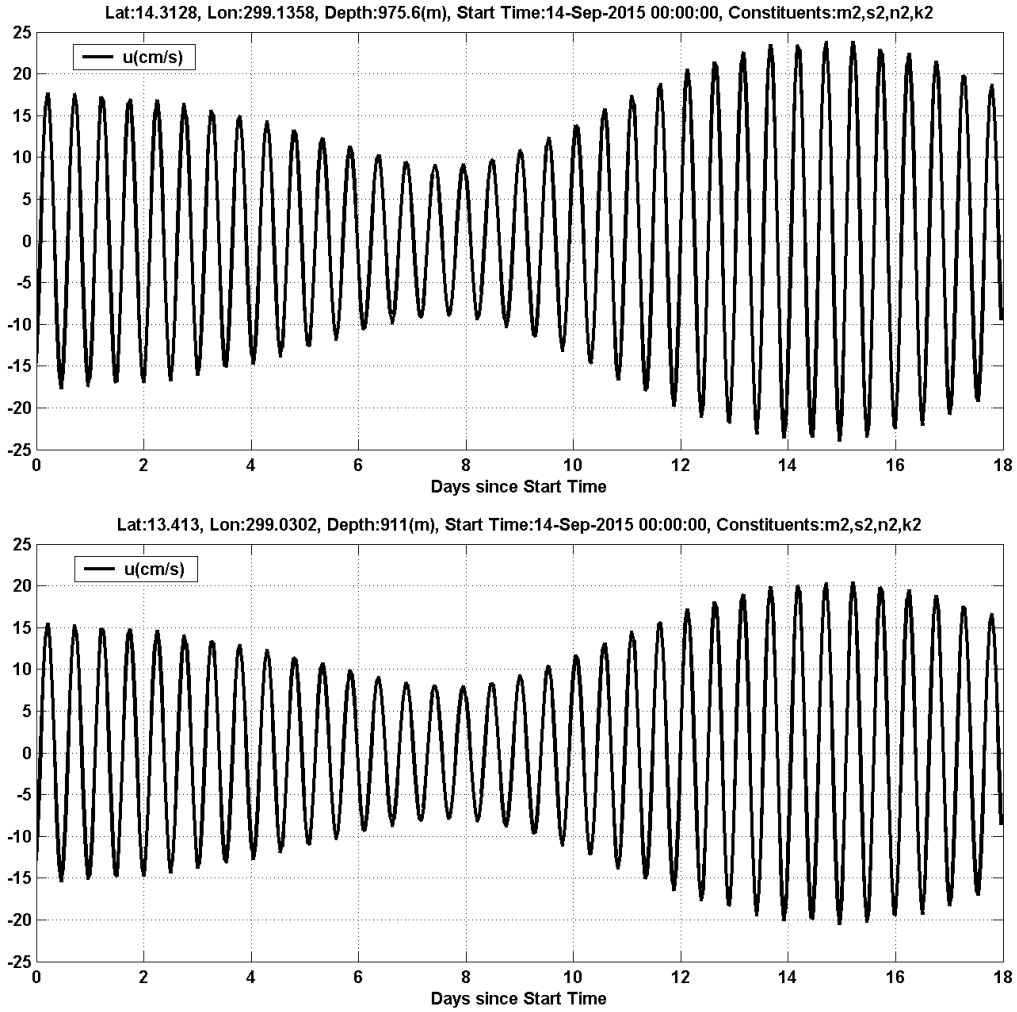

Figure 4 – The zonal (East-West) component of current speed (cm/s) at St. Lucia Passage (top) and St. Vincent Passage (bottom) starting during apogee-spring tides (14-SEP-2015). On day 14.708 (28-SEP-2015 17:00) were the perigee-spring tides.

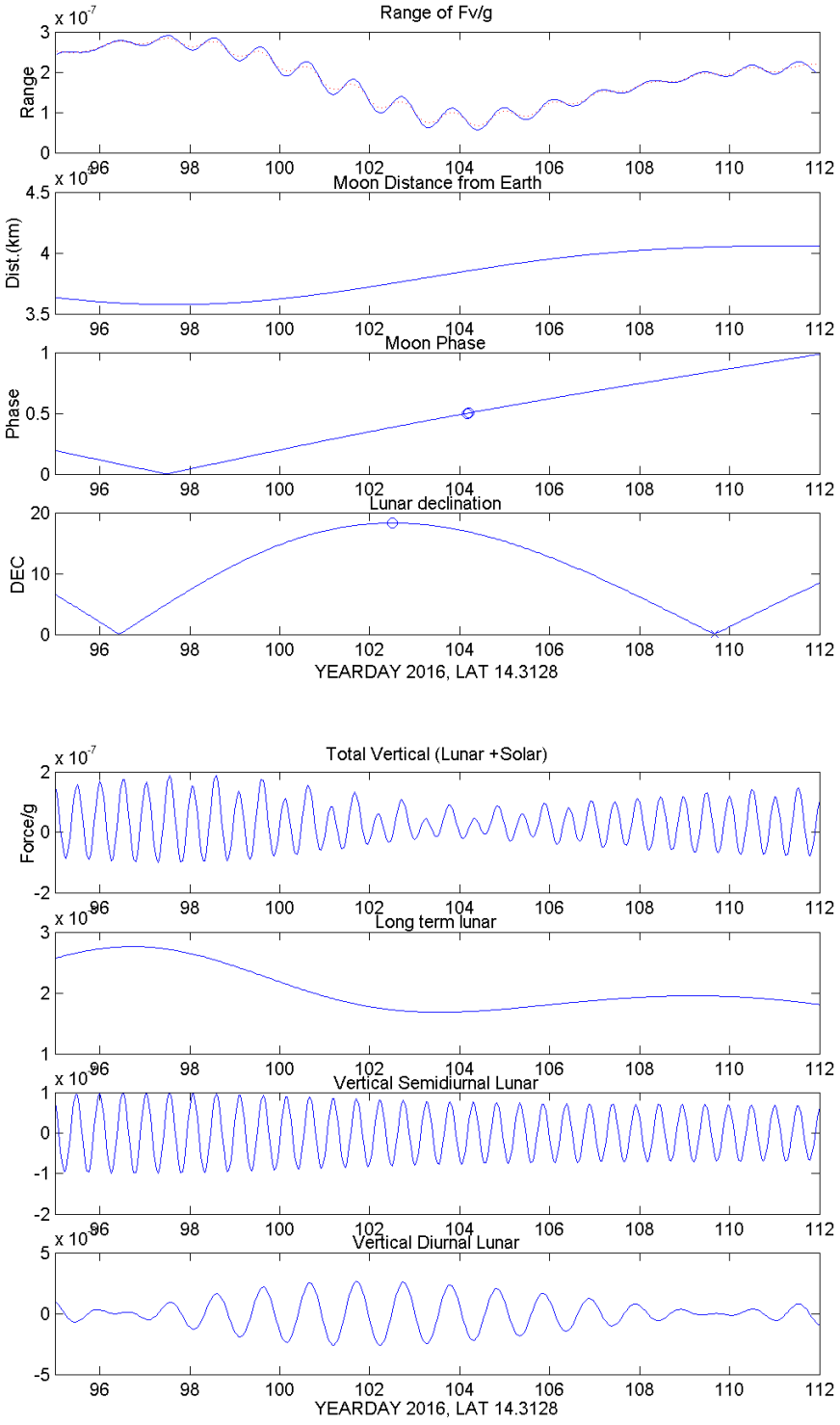

Figure 5 – (Top) Range of the total vertical luni-solar acceleration, Geocentric Moon's distance from Earth, Moon's phase and lunar declination. (Bottom) Total vertical luni-solar acceleration, vertical long-term lunar acceleration, vertical semidiurnal lunar acceleration and vertical diurnal lunar acceleration.

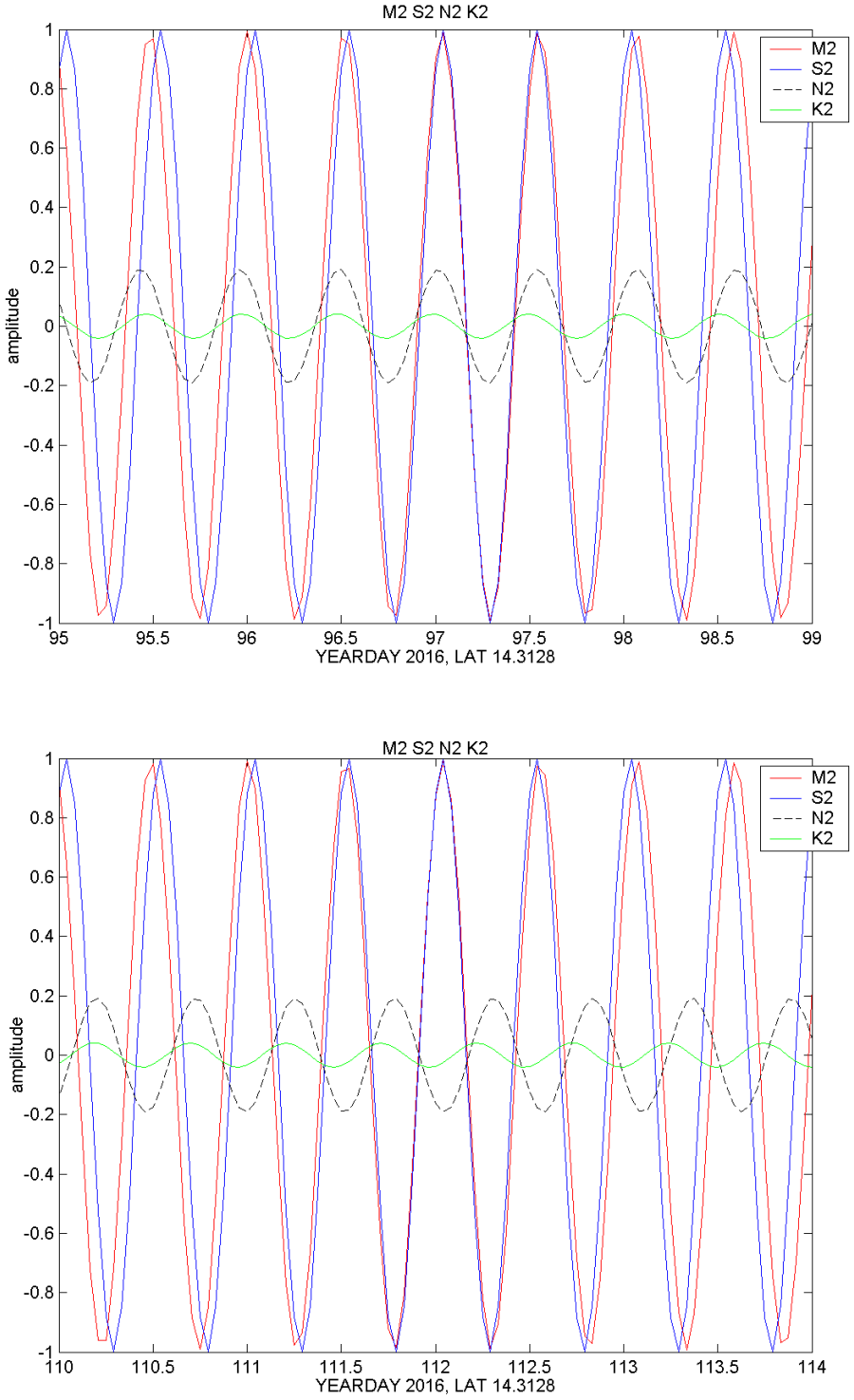

Figure 6 - The semidiurnal constituents of the vertical acceleration. The amplitudes were normalized for an easier comparison. The year day 97 and 112 of 2016 are equivalent to 7-APR-2016 and 22-APR-2016.

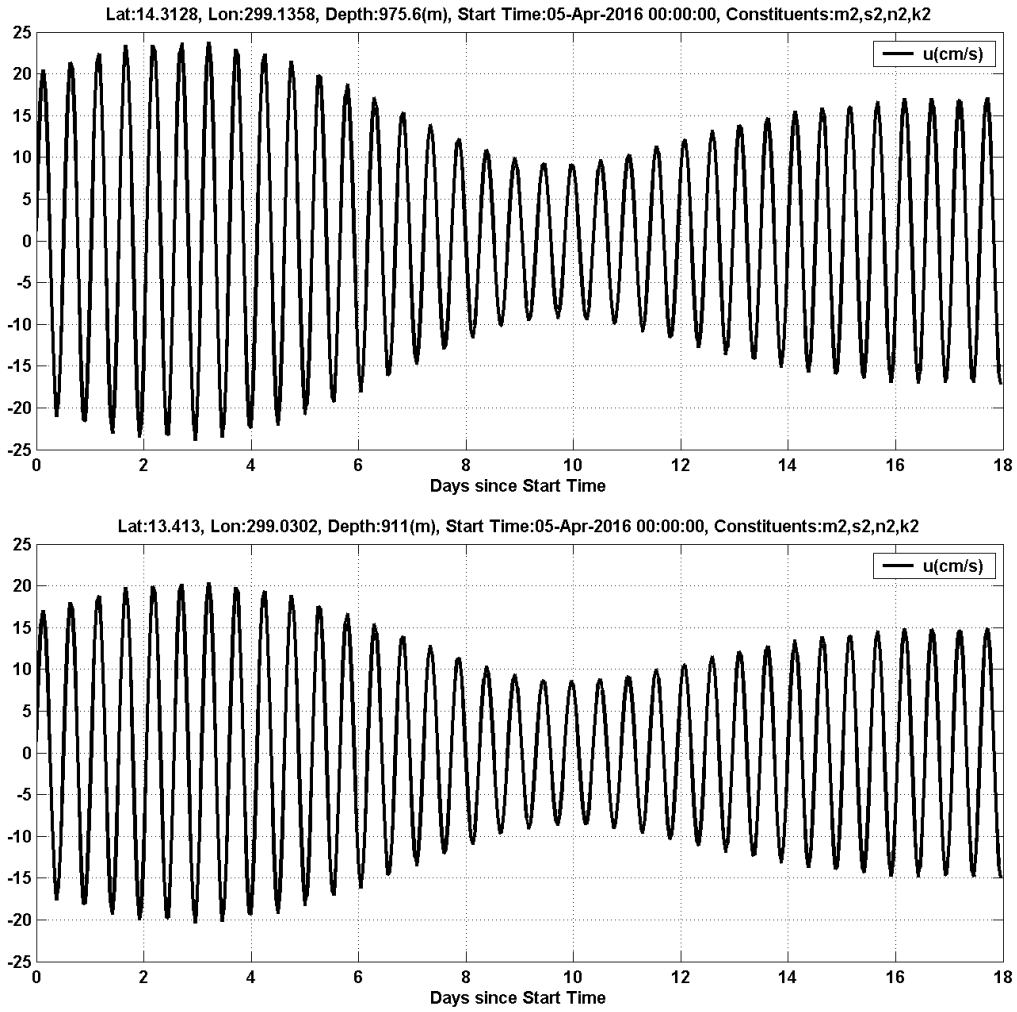

Figure 7 – The zonal (East-West) component of current speed (cm/s) at St. Lucia Passage (top) and St. Vincent Passage (bottom) starting on 5-APR-2016. On day 3.207 (8-APR-2016 4:58) were the perigee-spring tides and on day 16.664 (21-APR-2016 15:56) were the apogee-spring tides.

Source Location	component of current	Lat	Lon	Depth (m)	Day Since Start Time	Date	Apogee-Spring Currents (cm/s)	Day Since Start Time	Date	Perigean-Spring Currents (cm/s)	Percentage Change from Perigean-Spring to Apogee-Spring currents (%)	Percentage Change from Squared Perigean-Spring to Squared Apogee-Spring currents (%)	Dissipation Location
Brasil Shelf Break 1	v	1.3395	313.46	199.2	1.0463	9/15/2015 1:06	7.9	14.5038	9/28/2015 12:05	10.2	-23.1	-40.8	W. Equatorial Atlantic O.
Brasil Shelf Break 2	v	0.95077	313.8636	196.9	1.0463	9/15/2015 1:06	13.9	14.5038	9/28/2015 12:05	18.1	-23.1	-40.9	W. Equatorial Atlantic O.
Luzon Strait	u	20.1071	121.8356	536.2	1.2845	9/15/2015 6:49	38.6	14.742	9/28/2015 17:48	50.2	-23.2	-41.0	South China Sea
Nicobar Islands	u	8.8376	92.7648	209.8	1.0463	9/15/2015 1:06	19.4	15.0482	9/29/2015 1:09	24.6	-20.9	-37.5	Bay of Bengal
Sape Strait	v	-8.6686	119.3048	199.7	1.7439	9/15/2015 17:51	165.4	16.7495	9/30/2015 17:59	210.3	-21.3	-38.1	Indian Ocean
Sape Strait NE	v	-8.3951	119.3911	225.8	2.2543	9/16/2015 6:06	93.6	16.7495	9/30/2015 17:59	117.8	-20.5	-36.8	Indian Ocean
St. Lucia Passage	u	14.3128	299.1358	975.6	0.2127	9/14/2015 5:06	17.7	14.7079	9/28/2015 16:59	23.7	-25.6	-44.6	Eastern Caribbean Sea
St. Vincent Passage	u	13.413	299.0302	911	0.2127	9/14/2015 5:06	15.4	14.7079	9/28/2015 16:59	20.3	-24.0	-42.2	Eastern Caribbean Sea
Sibutu Passage	v	4.7819	119.6922	277.5	0.5359	9/14/2015 12:51	70.3	15.0482	9/29/2015 1:09	86.0	-18.3	-33.2	Celebes Sea
Lombok Strait	v	-8.7312	115.7476	297.1	1.7439	9/15/2015 17:51	138.3	16.7495	9/30/2015 17:59	179.4	-22.9	-40.6	Indian Ocean
Ombai Strait	v	-8.2728	125.4684	577.3	1.2505	9/15/2015 6:00	49.3	16.2561	9/30/2015 6:08	61.3	-19.5	-35.2	Banda Sea
										Average	**-22.0**	**-39.2**	
Edwin Alfonso-Sosa (2016)										STD	2.1	3.3	

Source Location	component of current	Lat	Lon	Depth (m)	Day Since Start Time	Date	Apogee-Spring Currents (cm/s)	Day Since Start Time	Date	Perigean-Spring Currents (cm/s)	Percentage Change from Perigean-Spring to Apogee-Spring currents (%)	Percentage Change from Squared Perigean-Spring to Squared Apogee-Spring currents (%)	Dissipation Location
Brasil Shelf Break 1	v	1.3395	313.46	199.2	17.5151	4/22/16 12:21	7.7	2.4924	4/7/16 11:49	10.1	-23.9	-42.1	W. Equatorial Atlantic O.
Brasil Shelf Break 2	v	0.95077	313.8636	196.9	17.0047	4/22/16 0:06	13.7	2.4924	4/7/16 11:49	17.9	-23.4	-41.4	W. Equatorial Atlantic O.
Luzon Strait	u	20.1071	121.8356	536.2	17.2429	4/22/16 5:49	37.0	2.7476	4/7/16 17:56	50.2	-26.3	-45.7	South China Sea
Nicobar Islands	u	8.8376	92.7648	209.8	17.5321	4/22/16 12:46	18.3	3.0369	4/8/16 0:53	24.6	-25.5	-44.5	Bay of Bengal
Sape Strait	v	-8.6686	119.3048	199.7	17.7023	4/22/16 16:51	154.2	4.7552	4/9/16 18:07	208.4	-26.0	-45.3	Indian Ocean
Sape Strait NE	v	-8.3951	119.3911	225.8	17.7023	4/22/16 16:51	86.9	5.2486	4/10/16 5:57	117.8	-26.2	-45.5	Indian Ocean
St. Lucia Passage	u	14.3128	299.1358	975.6	16.6645	4/21/16 15:56	17.1	3.207	4/8/16 4:58	23.7	-28.0	-48.1	Eastern Caribbean Sea
St. Vincent Passage	u	13.413	299.0302	911	16.1711	4/21/16 4:06	14.9	3.207	4/8/16 4:58	20.2	-26.4	-45.8	Eastern Caribbean Sea
Sibutu Passage	v	4.7819	119.6922	277.5	17.5491	4/22/16 13:10	67.7	3.0369	4/8/16 0:53	85.6	-21.0	-37.5	Celebes Sea
Lombok Strait	v	-8.7312	115.7476	297.1	17.7193	4/22/16 17:15	128.6	4.7722	4/9/16 18:31	178.7	-28.0	-48.2	Indian Ocean
Ombai Strait	v	-8.2728	125.4684	577.3	17.7023	4/22/16 16:51	45.8	4.7552	4/9/16 18:07	61.3	-25.4	-44.3	Banda Sea
										Average	**-25.5**	**-44.4**	
Edwin Alfonso-Sosa (2016)										STD	2.1	3.1	

Table 2 – Summary of maximum speed of currents during perigee-spring tides versus apogee-spring tides and its percentage change at each of the selected locations.

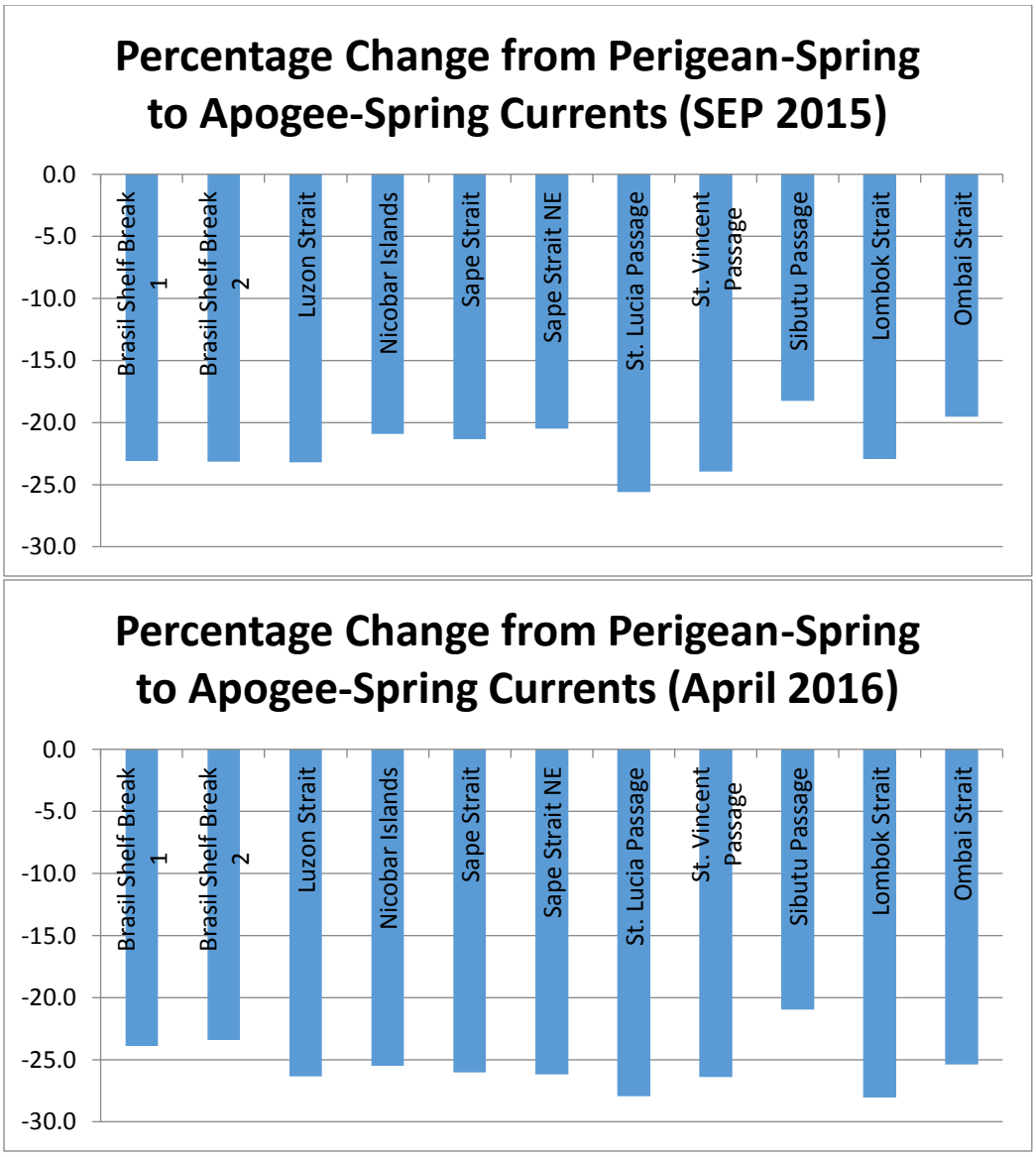

Figure 8 – Percentage change from perigee-spring to apogee-spring tidal currents on September 2015 and on April 2016.

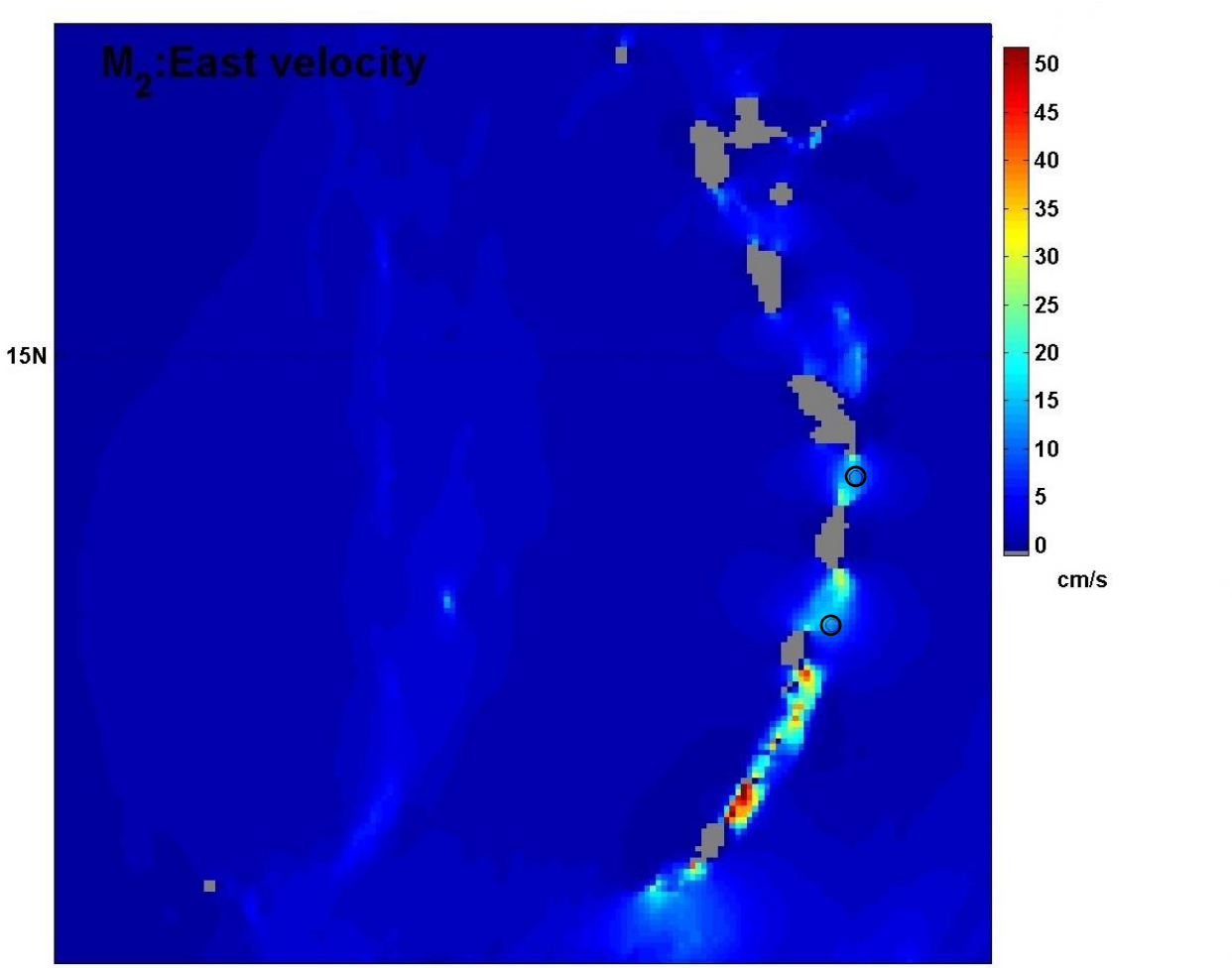

Figure 9 - East velocity of the M2 tidal currents through the Lesser Antilles passages. The St. Lucia and St. Vincent Passages are identified with black circles.

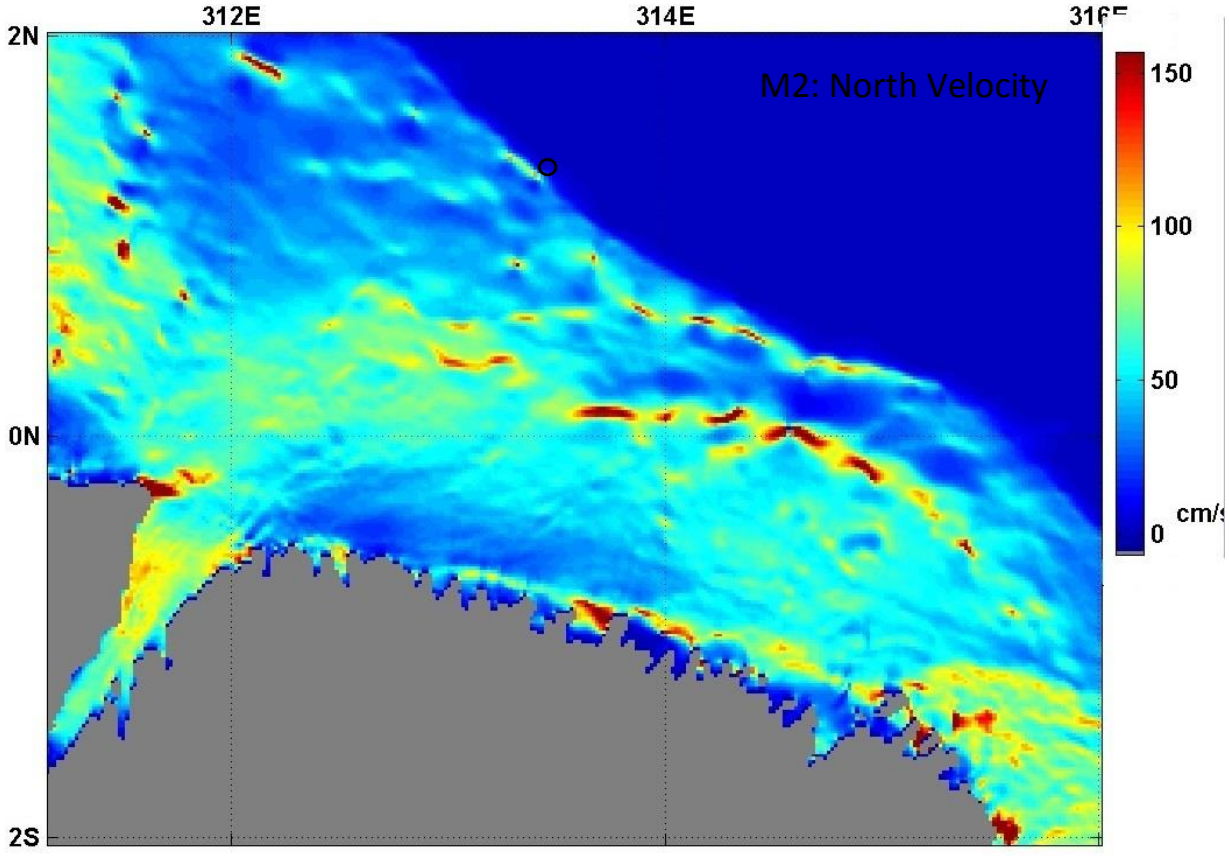

Figure 10 - North velocity of the M2 tidal currents in the northeastern Brazil continental shelf, offshore the Amazon Delta. The black circle marks the location of Brazil Shelf Break 1.

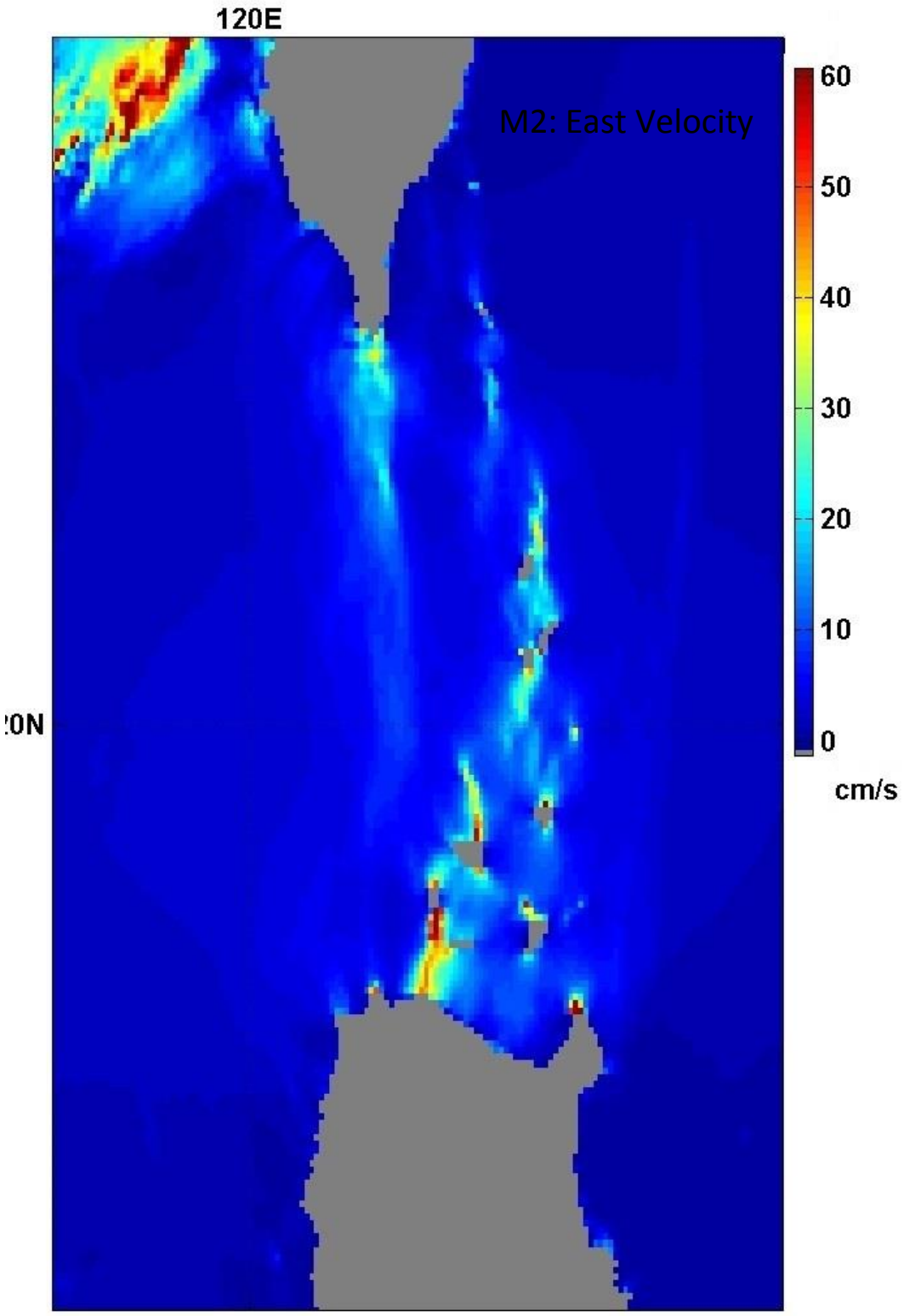

Figure 11 - East velocity of the M2 tidal currents through the Luzon Strait.

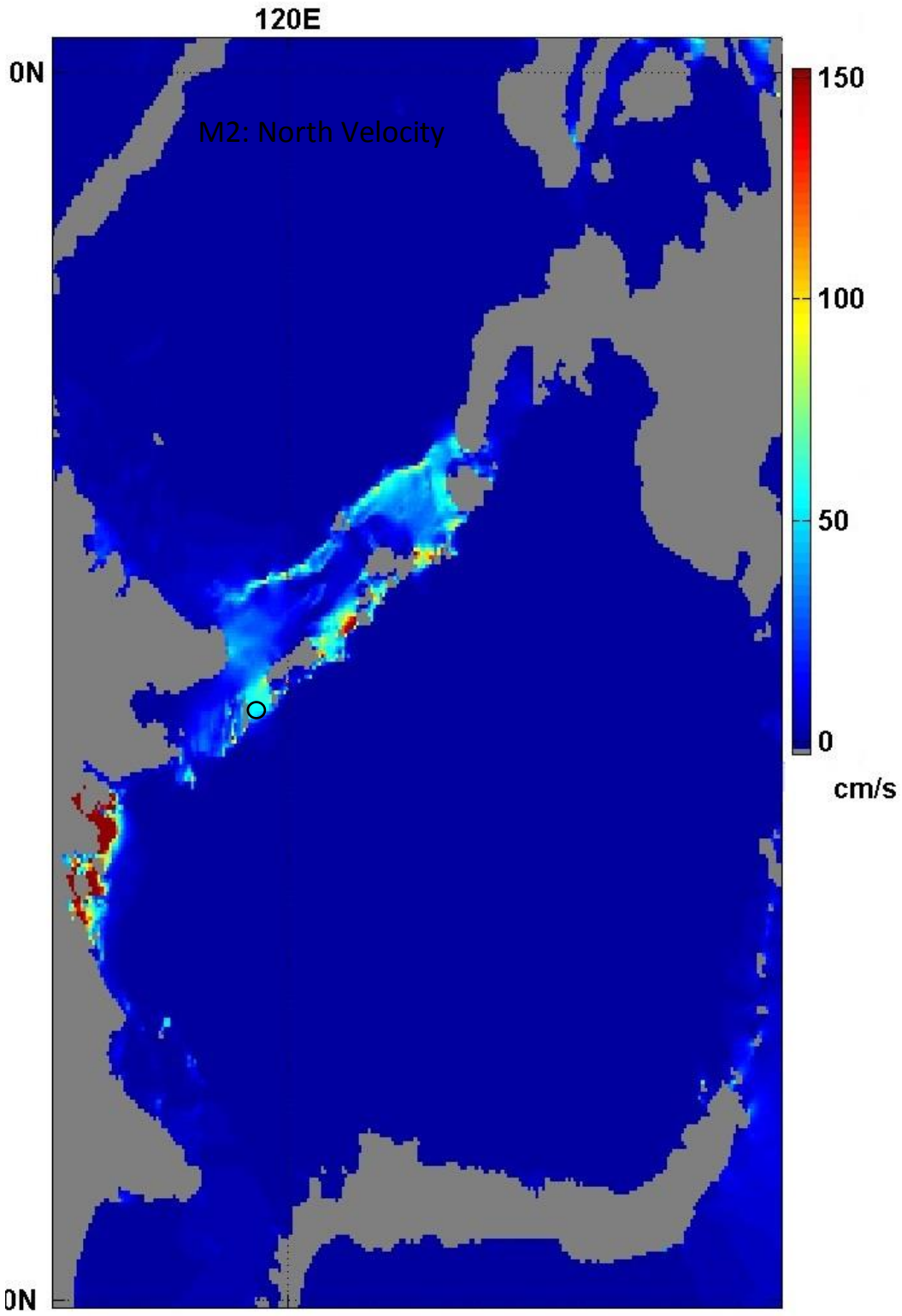

Figure 12 - North velocity of the M2 tidal currents through the Sibutu Strait (black circle).

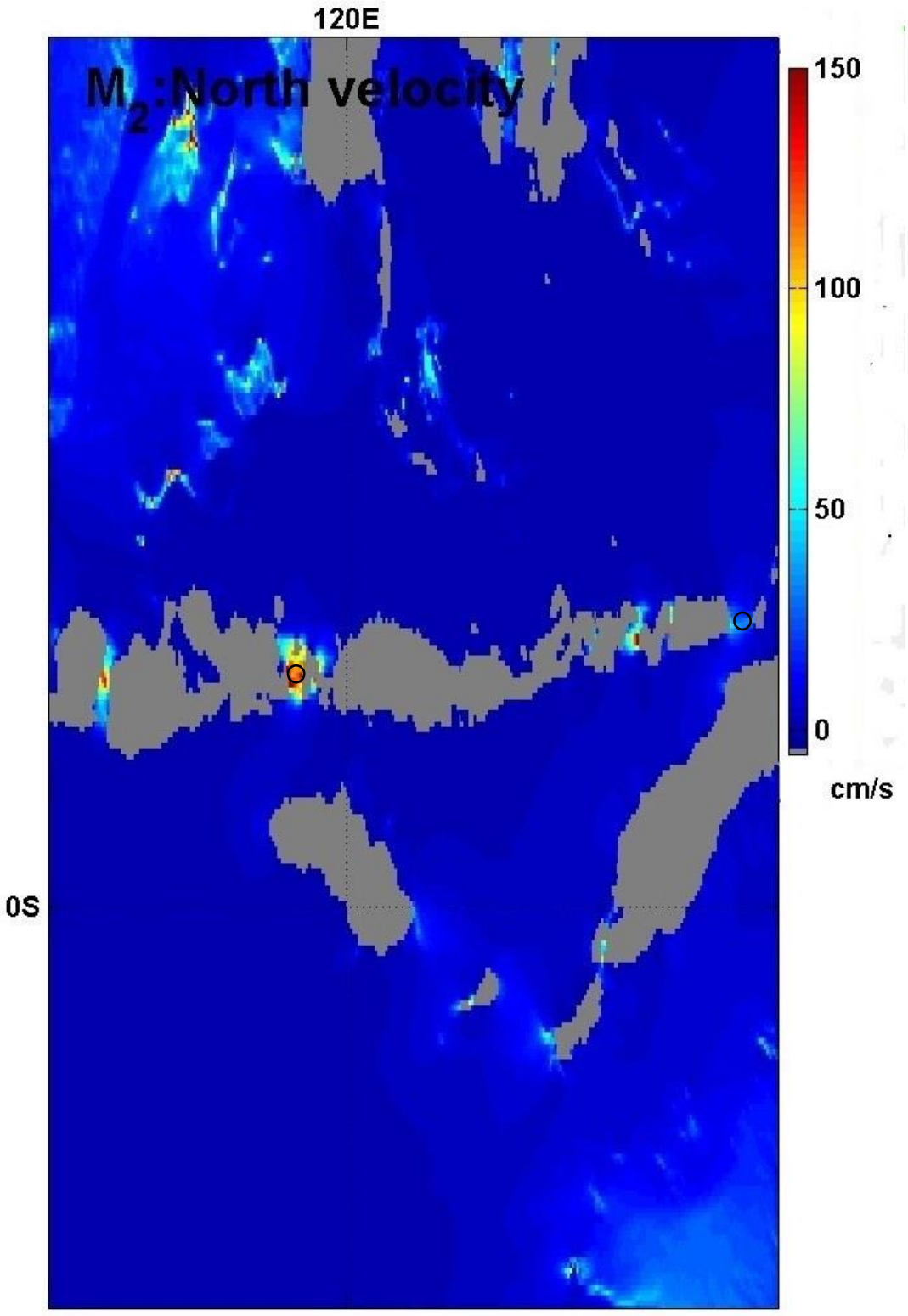

Figure 13 - North velocity of the M2 tidal currents through the Indonesian straits. The black circles mark the location of Sape Strait (left) and Ombai Strait (right).

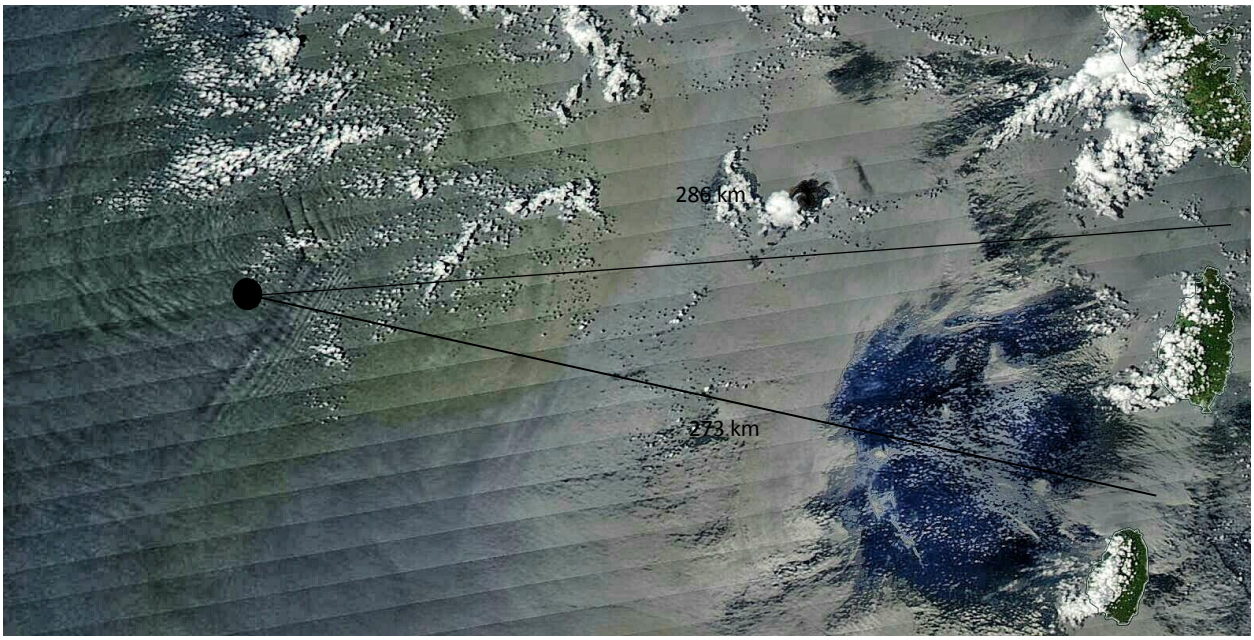

Figure 14 – Two packets of internal solitary waves converge about 19 km east of the Aves Ridge. Strong semidiurnal currents during perigee-spring tides occurred on St. Lucia and St. Vincent passages; the two passages are almost equidistant from the Aves Ridge. Image captured by MODIS/Aqua on 28-SEP-2015.

Figure 15 – Internal waves travelling northeast were generated at the Brazil shelf break. Image captured by MODIS/Terra on 27-SEP-2015.

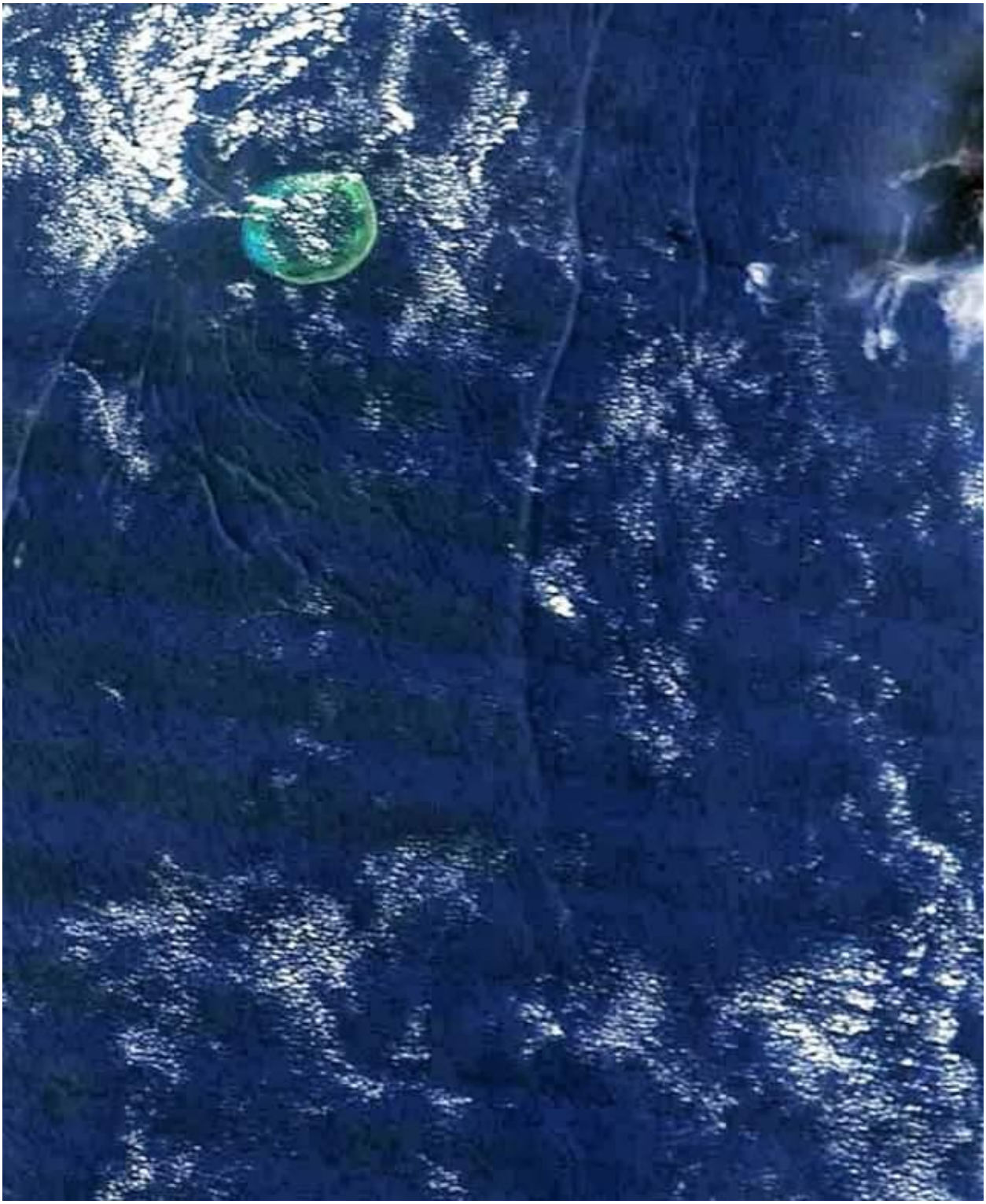

Figure 16 Internal solitary waves generated at Luzon Strait are travelling west toward the Dongsha Atoll. Image captured by MODIS/Terra on 01-OCT-2015.

Figure 17 – Internal solitary waves generated at Sibutu Strait are travelling southeast in the Celebes Sea. Image captured by MODIS/Terra on 30-SEP-2015.

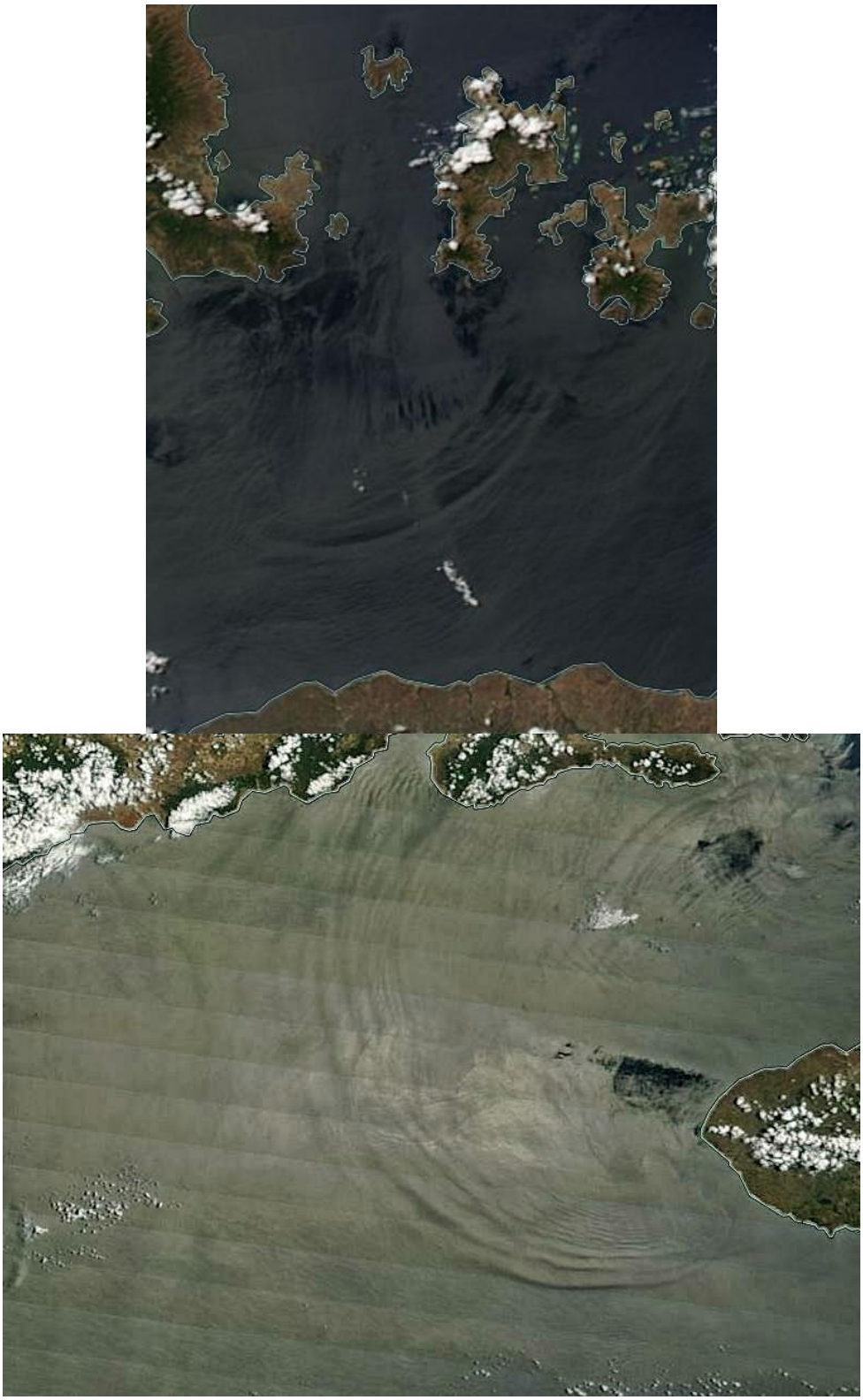

Figure 18 – Internal solitary waves generated at Sape Strait travelling south toward Sumba Island (top) and travelling southwest along the Sumba Strait toward the Indian Ocean (bottom). Image captured by MODIS/Terra on 30-SEP-2015.

Source Location	Start	First Detection	Last Detection	End	Undetected	IW detections by MODIS from 9 to 17 SEP 2015	Days between last and first IW detection (from 9 to 17 SEP 2015)	Start	First Observed	Last Observed	End	Undetected	IW detections by MODIS from 26-SEP to 4-OCT 2015	Days between last and first IW detection (from 26-SEP to 4-OCT 2015)
Brasil Shelf Break	9-Sep-15	15-Sep-15	15-Sep-15	17-Sep-15	15	1	0	26-Sep-15	27-Sep-15	1-Oct-15	4-Oct-15	12	4	4
Luzon Strait	9-Sep-15	16-Sep-15	17-Sep-15	17-Sep-15	14	2	1	26-Sep-15	1-Oct-15	1-Oct-15	4-Oct-15	15	1	0
Nicobar Islands	9-Sep-15	14-Sep-15	14-Sep-15	17-Sep-15	15	1	0	26-Sep-15	2-Oct-15	2-Oct-15	4-Oct-15	15	1	0
Sape Strait	9-Sep-15	12-Sep-15	16-Sep-15	17-Sep-15	11	5	4	26-Sep-15	28-Sep-15	4-Oct-15	4-Oct-15	7	9	6
St. Lucia Passage	9-Sep-15	13-Sep-15	17-Sep-15	17-Sep-15	14	2	4	26-Sep-15	27-Sep-15	4-Oct-15	4-Oct-15	10	6	7
Sibutu Passage	9-Sep-15	14-Sep-15	14-Sep-15	17-Sep-15	15	1	0	26-Sep-15	30-Sep-15	4-Oct-15	4-Oct-15	13	3	4
Lombok Strait	9-Sep-15	14-Sep-15	14-Sep-15	17-Sep-15	14	2	0	26-Sep-15	28-Sep-15	3-Oct-15	4-Oct-15	10	6	5
Ombai Strait	9-Sep-15	13-Sep-15	16-Sep-15	17-Sep-15	13	3	3	26-Sep-15	29-Sep-15	4-Oct-15	4-Oct-15	9	7	5
Edwin Alfonso-Sosa (2016)														

Table 3 – Internal wave detections by MODIS around perigee-spring tides versus apogee-spring tides and the number of days passed between last and first detection.

Source Location	Start	First Detection	Last Detection	End	Undetected	IW detections by MODIS from 4 to 12 APR 2016	Days between last and first IW detection (from 4 to 12 APR 2016)	Start	First Observed	Last Observed	End	Undetected	IW detections by MODIS from 19 to 27 APR 2016	Days between last and first IW detection (from 19 to 27 APR 2016)
Brasil Shelf Break	4-Apr-16	6-Apr-16	8-Apr-16	12-Apr-16	14	2	2	19-Apr-16	24-Apr-16	24-Apr-16	27-Apr-16	15	1	0
Luzon Strait	4-Apr-16	6-Apr-16	12-Apr-16	12-Apr-16	10	6	6	19-Apr-16	21-Apr-16	27-Apr-16	27-Apr-16	10	6	6
Nicobar Islands	4-Apr-16	4-Apr-16	12-Apr-16	12-Apr-16	9	7	8	19-Apr-16	19-Apr-16	27-Apr-16	27-Apr-16	9	7	8
Sape Strait	4-Apr-16	9-Apr-16	9-Apr-16	12-Apr-16	13	3	0	19-Apr-16	23-Apr-16	27-Apr-16	27-Apr-16	12	4	4
St. Lucia Passage	4-Apr-16	5-Apr-16	12-Apr-16	12-Apr-16	13	3	7	19-Apr-16	0-Jan-00	0-Jan-00	27-Apr-16	16	0	0
Sibutu Passage	4-Apr-16	9-Apr-16	11-Apr-16	12-Apr-16	13	3	2	19-Apr-16	23-Apr-16	27-Apr-16	27-Apr-16	13	3	4
Lombok Strait	4-Apr-16	5-Apr-16	12-Apr-16	12-Apr-16	12	4	7	19-Apr-16	21-Apr-16	25-Apr-16	27-Apr-16	11	5	4
Ombai Strait	4-Apr-16	8-Apr-16	8-Apr-16	12-Apr-16	15	1	0	19-Apr-16	22-Apr-16	27-Apr-16	27-Apr-16	12	4	5
Edwin Alfonso-Sosa (2016)														

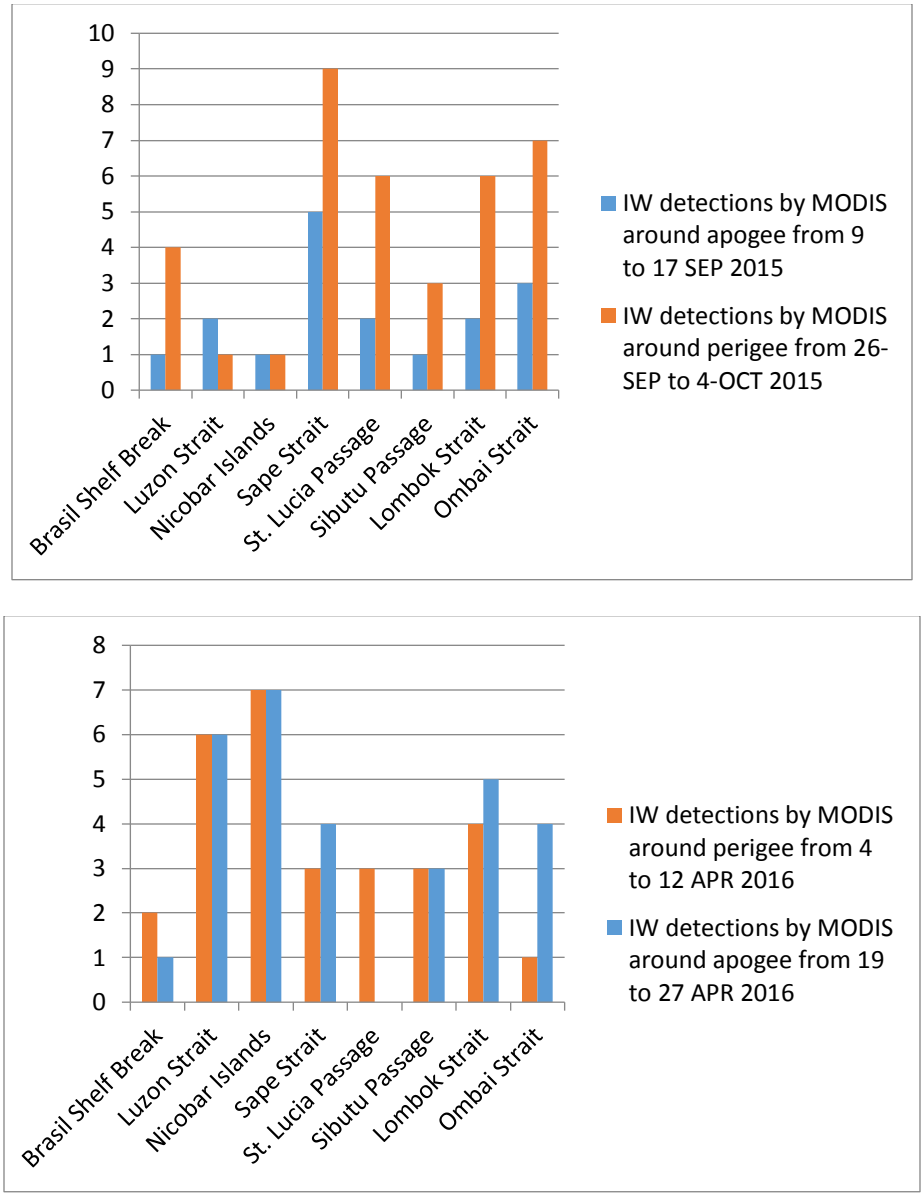

Figure 19 - Internal wave detections by MODIS around perigee-spring tides versus apogee-spring tides.

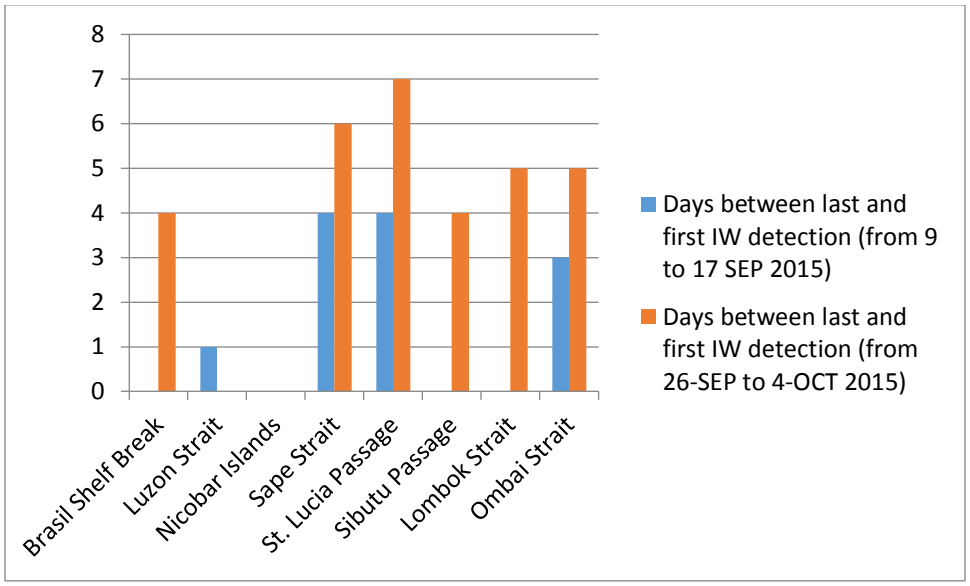

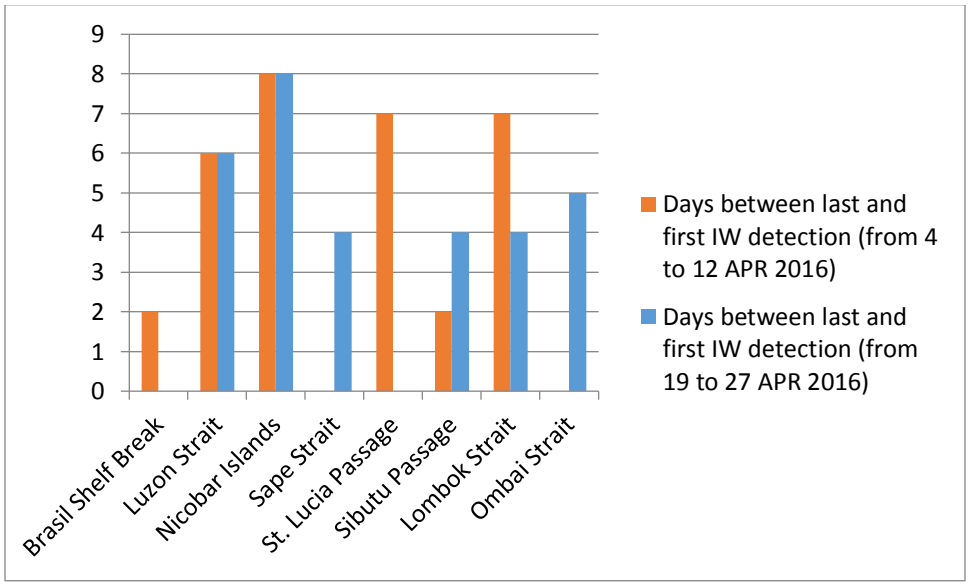

Figure 20 – Elapsed days between last and first detection around perigee-spring tides versus apogee-spring tides.

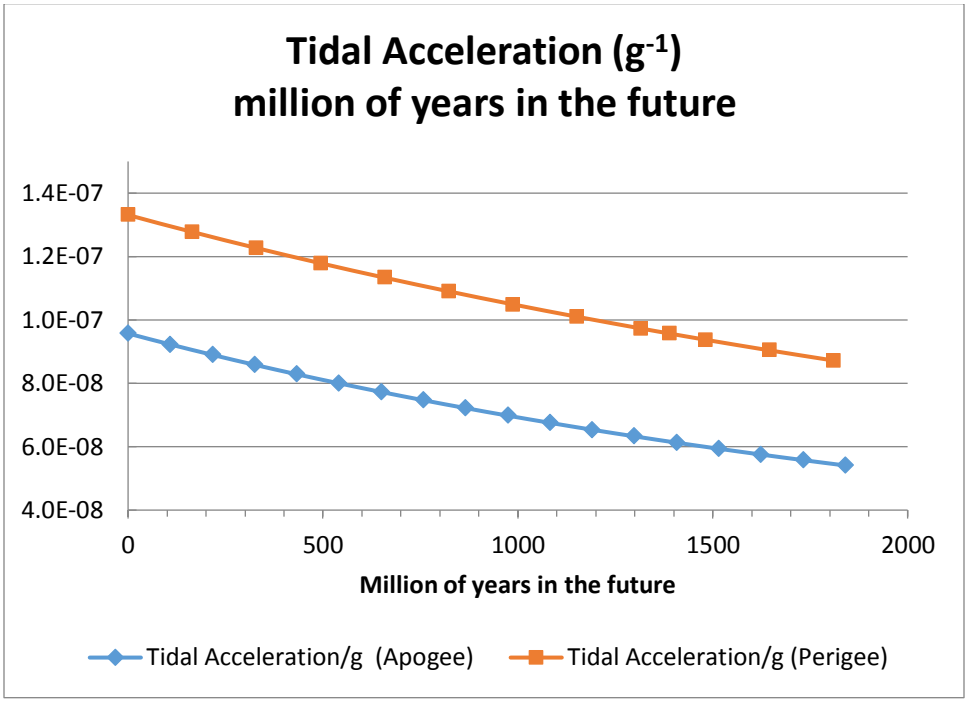

Figure 21- Projection of the tidal acceleration millions of years into the future. Blue is during apogee and red during perigee.

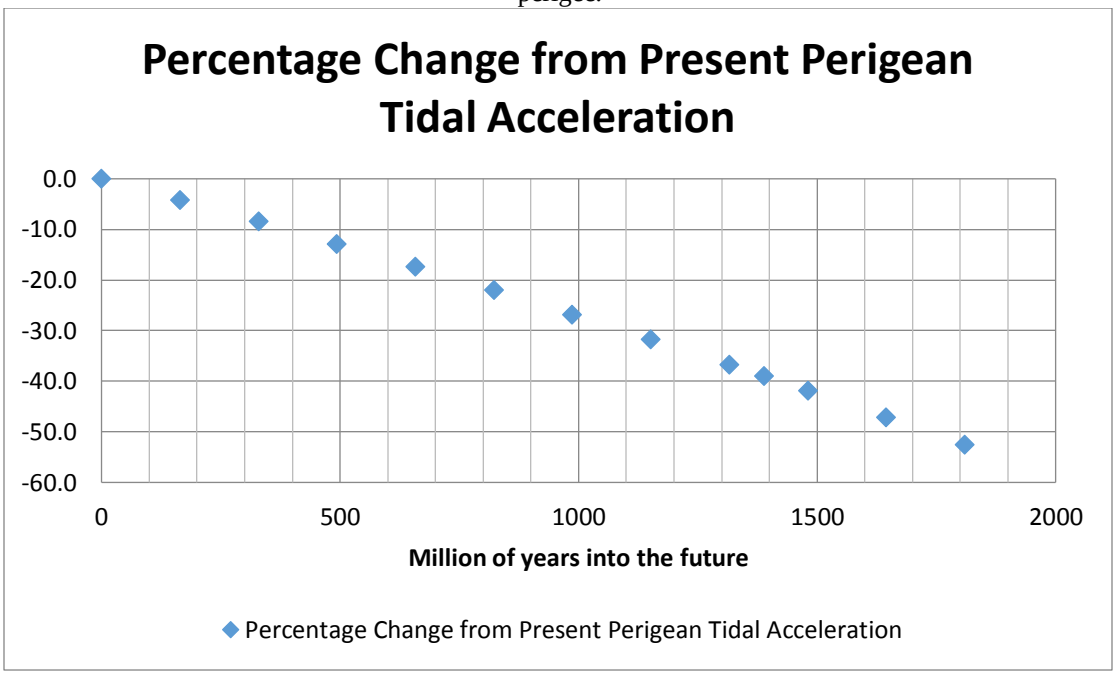

Figure 22- Percentage change from present perigee tidal acceleration.